Piezoelectric Performance of Electrospun PVDF and PVDF-composite Fibers: A Review and Machine Learning Based Analysis

Jiawei Chen[1], Cagri Ayranci[*], and Tian Tang[*]
Department of Mechanical Engineering, University of Alberta, 116 St & 85 Ave, Edmonton, Alberta, Canada
[*]Corresponding Author: tian.tang@ualberta.ca; cayranci@ualberta.ca; Tel: +1 780 492 5467 Tel: +1 780 492 2791

Keywords: Energy materials; Polymer (textile) fibres; Electrospinning; Machine Learning

Abstract

The development of polyvinylidene fluoride (PVDF) fibers via electrospinning has driven the research of piezoelectric materials towards applications in self-powered generators with superior flexibility, great biocompatibility, and high electric output. In the last decade, many studies have been conducted on improving the piezoelectric properties of electrospun PVDF fibers by introducing fillers or additives. In this work, studies that produced and characterized electrospun PVDF and PVDF composite fibers were summarized. Machine learning (ML) was used to analyze existing data and establish models that can predict the piezoelectric output of PVDF composite fibers from material and synthesis parameters with good accuracy. This work provides extensive review and unique perspectives on the current advancements and challenges in using fillers to enhance the flexibility and piezoelectricity of PVDF fibers, an approach that bears great potential in the field of high-performance energy harvesting systems.

1. Introduction

As the depletion of natural resource accentuates the significance to seek innovative and green methods in energy harvesting, self-powered generators, especially in the nano-scale, have gained increasing research interests. Generating electrical charges in the absence of an external electrical power source, a self-powered generator can be based on piezoelectricity, which converts mechanical energy into electrical energy [1,2]. Significant research work has been devoted to piezoelectric materials in recent years to harvest ambient kinetic energy. Piezoelectric materials refer to the substances with crystal structures that can undergo expansion or contraction in response to an applied electric field [3]. Conversely, as the crystal structure of such a material experiences deformation, separation of charge generates a dipole moment so that an electric energy can be produced. The broad application of piezoelectric materials ranges from pressure transducer for health monitoring of large-scale equipment such as airplanes to nano-electromechanical systems like nano-actuators or nano-sensors [4,5]. Piezoelectric materials can be embedded in wearable accessories to convert human motion into electric energy as schematically shown in Figure 1. Due to its tailorable dimension and functionality, exploring the full potential of piezoelectric materials in energy harvesting is paramount to the development of next-generation power systems.

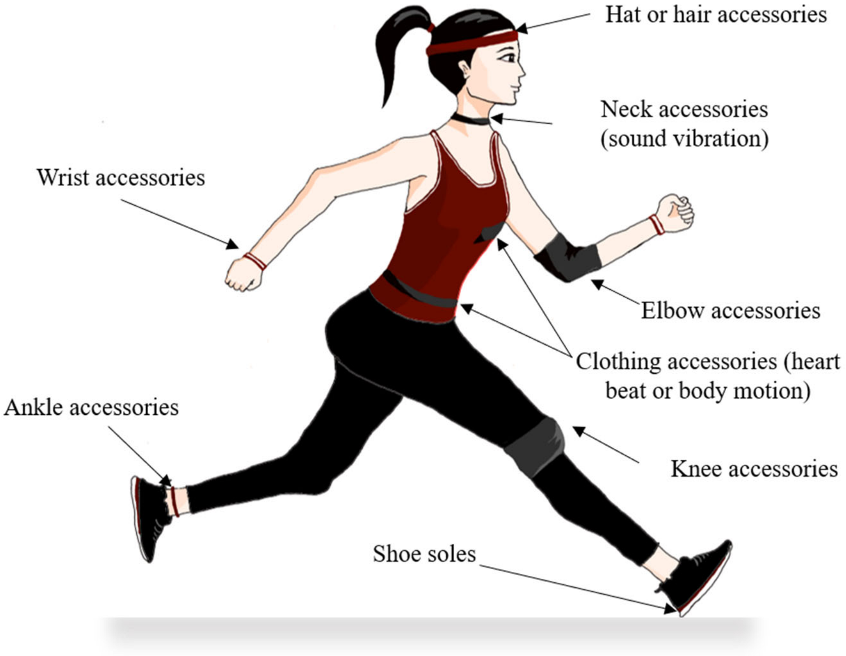

Figure 1. Piezoelectric materials embedded in wearable accessories to harvest energy from human motion.

There are two major groups of piezoelectric materials, piezoelectric ceramics and piezoelectric polymers. Piezoelectric ceramics are more available commercially owing to their superior piezoelectricity and dielectric properties. Commercial piezoelectric ceramics, which are mostly Lead Zirconate Titanate (PZT)-based, are widely used as gas igniters, sensors, low frequency actuators, etc. [6] Despite the fact that piezoelectric ceramics present high sensitivity in generator or sensor applications, processing of piezoelectric ceramics typically involves high energy consumption such as sintering at 1200-1300℃, followed by poling, or exposure to high electric field to orient the crystal structures [7]. Additionally, brittleness restricts piezoelectric ceramics from applications that require flexibility or high ductility. Because of these limitations, studies in recent years are steered more towards piezoelectric polymers, which are lighter and possess far higher flexibility.

Among various piezoelectric polymers, Polyvinylidene Fluoride (PVDF) family has dominated the research field due to its good piezoelectric property, ease of fabrication, and high flexibility. PVDF-derived polymers include its copolymers such as Polyvinylidene Fluoride-Trifluoroethylene (PVDF-TrFE) or Polyvinylidene Fluoride-Hexafluoropropylene (PVDF-HFP), and its terpolymers such as Polyvinylidene Fluoride-Trifluoroethylene-Chlorotrifluoroethylene (PVDF-TrFE-CTFE) [8]. PVDF fiber has garnered considerable attention in the manufacturing of functional piezoelectric devices or structures. For instance, in the area of electronic textiles or e-textiles, which are fabrics embedded with electronic functionality, lightweight PVDF fibers can be fabricated into yarns with average diameter of ~60 µm, which are subsequently woven into textiles for energy harvesting from human motion [9]. In biomedical applications, biocompatible PVDF fibers with high flexibility and small diameter (~110 nm) can convert cardiac motion into electrical energy for powering heart pacemaker [10]. To enable similar nano-scale applications such as flexible nanogenerators or nano-sensors, the size of the PVDF fibers can be reduced by adopting a processing method called electrospinning [11]. Growing amount of research has focused on improving the voltage output of the PVDF fibers produced by electrospinning. Addition of fillers is one method to enhance the piezoelectric properties.

As such, this work presents an overview of the parameters that affect the piezoelectric performance of electrospun PVDF and PVDF composite fibers, their characterizations, and usage of fillers for piezoelectricity improvement. In addition, a machine learning (ML) analysis is conducted on the published data in recent 10 years, to investigate and predict the output voltage of electrospun PVDF composite fibers reinforced with various fillers.

2. PVDF Fibers

2.1. PVDF

Reported first by Heiji Kawai in 1969 [12], PVDF is a semicrystalline fluoropolymer with stable piezoelectric responses and high piezoelectric coefficients surpassing most other thermoplastic polymers. PVDF-based polymers exhibit large energy density (up to ~30 J/cm^3), high dielectric constant (~12), great biocompatibility, robust mechanical properties, and high thermal stability [13,14]. Polymerization of the monomer unit $H_2C{=}CF_2$ forms the molecular chain of PVDF with several crystalline polymorphs: α, β, γ, δ, and ε phases. The α phase is non-polar or non-piezoelectric, but due to its high thermal stability, without any treatment this is the general crystallite form of PVDF. The β phase has the highest degree of spontaneous polarization and thus higher piezoelectricity and ferroelectricity than other phases. The γ phase is also electroactive with excellent energy storage capacity, but it has lower piezoelectricity and higher melting temperature than the β phase [15]. The δ phase is the polar form of the α phase with every second chain twisted 180° [16]. The ε phase is the non-polar analogue of the γ phase [17]. The α, β, and γ phases attract most research attention as they are the three most common crystalline forms of PVDF. The molecular conformation of these crystalline phases is trans-gauche (TGTG’) for α phase, all-trans (TTTT) zigzag planar for β phase, and three trans-one gauche (TTTGTTTG’) for γ phase as shown in Figure 2. Typically, α phase can be achieved by reducing temperature from the molten state, β phase by mechanical stretching, and γ phase by high-temperature or solution-inducing crystallization [18]. The conversion of the non-polar α phase to the β phase which has the highest dipole moment generally involves mechanical stretching and poling. Mechanical stretching exerts a force on the molecular chain to extend the conformation into β phase while the electric field orients the dipole moments in the direction of the field to form β phase [17].

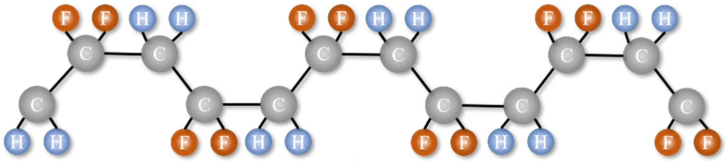

α phase

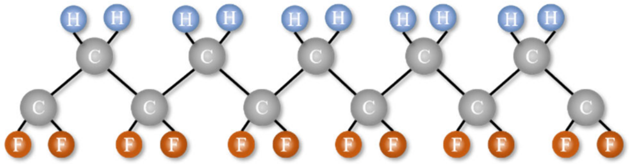

β phase

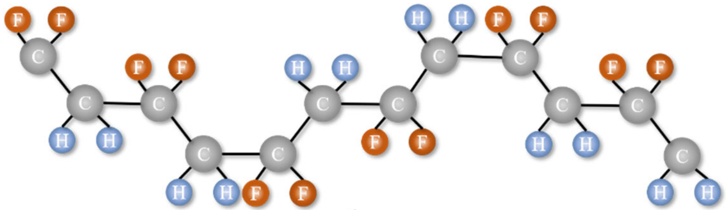

γ phase

Figure 2. Molecular conformations of α, β, and γ phases of PVDF chains.

2.2. Fiber fabrication

PVDF can be fabricated into different structures, such as membranes, fibers, and filaments. Fiber form of PVDF is of particular interest on account of its immense applications in biomedicine, cell scaffold, battery separator, etc. [19] Common production methods for PVDF fibers include melt spinning, wet spinning, dry spinning, and centrifugal spinning [20–22]. However, subsequent poling is required to convert α phase to an electroactive phase for the PVDF fibers to obtain piezoelectric properties. Electrospinning as the production method allows incorporation of poling in the manufacturing process to fabricate piezoelectric PVDF fibers. Two main electrospinning methods are solution electrospinning and melt electrospinning, which respectively produce fibers from a polymer solution and a polymer melt. In either method, liquidous PVDF that is discharged from a spinneret is subjected to a high electric field. Repulsion between the charges causes the liquid to overcome the surface tension and be stretched into a Taylor cone, and subsequently a stable and unstable polymer jet (Figure 3a) [23]. Under the electrostatic force, thinning of the travelled jet takes place and induces dipole reorientation of the PVDF chain, leading to the formation of the electroactive phase. Melt electrospinning does not involve toxic solvents but it is limited by low yield, more complicated equipment [24], and the thermal stability of the additives that can be used. For solution electrospinning, PVDF can be dissolved in dipolar aprotic solvents such as dimethyl sulfoxide (DMSO), dimethylformamide (DMF), Dimethylacetamide (DMAc) and acetone. During collection at the oppositely charged or grounded electrode, the solvent evaporates to yield electrospun PVDF fibers. Solution electrospinning has been reported more extensively due to more efficient production, easily tailorable fiber morphology and less restriction on apparatus requirement. On account of these desired characteristics, this review focuses on PVDF fibers produced by solution electrospinning.

Besides the ability to conduct in situ poling and stretching, another appealing feature of electrospinning compared to most other manufacturing methods is the production of ultrafine fiber mats with diameter of each fiber in the micrometer to nanometer range. Such fibers have large specific surface area and aspect ratio, and exhibit high piezoelectricity due to molecular chain orientation in the fiber direction which promotes the formation of electroactive crystallites. In addition, high flexibility of the thin fibers makes them suitable in applications such as e-textiles. Large porosity of the electrospun fiber mat also allows incorporation of fillers or functionalization that further enhances the piezoelectric performance [25].

To fabricate a generator or a device for testing, the electrospun PVDF fibers are generally sandwiched between two electrode layers, which are either coated with conductive materials or conductive foils, such as copper tapes or aluminum foils as shown in Figure 3b. Insulating layers are applied over the electrodes to reduce noise and pyroelectric effect arising from the temperature difference between the sample and the testing probe [26].

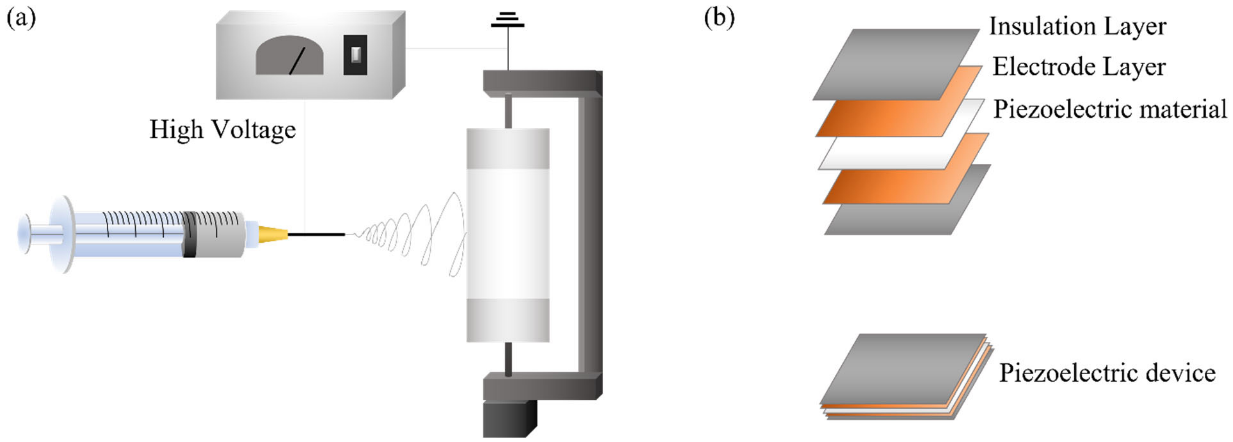

Figure 3. Schematics of (a) piezoelectric mat fabricated by solution electrospinning and (b) subsequent production of piezoelectric device.

3. Evaluation of Piezoelectric Properties

Diverse testing methods have been reported to characterize the piezoelectric properties of electrospun PVDF fibers. The characterization methods used recently are summarized below, along with some recommendations for more standardized procedures.

3.1. Piezoelectric coefficients

The piezoelectric behavior is governed by constitutive equations relating to stress, strain, electric field, and electric displacement in the material, according to the IEEE standard [27]. The constitutive equations are presented in strain-charge form, stress-charge form, strain-voltage form, and stress-voltage form as shown below,

$$\begin{array}{ll} \text{strain-charge form} & \text{stress-charge form} \\ \boldsymbol{\varepsilon} = \mathbf{s}_F \boldsymbol{\sigma} + \mathbf{d}^{\mathrm{T}} \mathbf{E} & \boldsymbol{\sigma} = \mathbf{c}_F \boldsymbol{\varepsilon} - \mathbf{e}^{\mathrm{T}} \mathbf{E} \\ \mathbf{D} = \mathbf{d} \boldsymbol{\sigma} + \boldsymbol{\kappa}_\sigma \mathbf{E} & \mathbf{D} = \mathbf{e} \boldsymbol{\varepsilon} + \boldsymbol{\kappa}_\varepsilon \mathbf{E} \\ \text{strain-voltage form} & \text{stress-voltage form} \\ \boldsymbol{\varepsilon} = \mathbf{s}_D \boldsymbol{\sigma} + \mathbf{g}^{\mathrm{T}} \mathbf{D} & \boldsymbol{\sigma} = \mathbf{c}_D \boldsymbol{\varepsilon} - \mathbf{h}^{\mathrm{T}} \mathbf{D} \\ \mathbf{E} = -\mathbf{g} \boldsymbol{\sigma} + \boldsymbol{\kappa}_\sigma^{-1} \mathbf{D} & \mathbf{E} = -\mathbf{h} \boldsymbol{\varepsilon} + \boldsymbol{\kappa}_\varepsilon^{-1} \mathbf{D} \end{array} \tag{1}$$

In the above equations, $\boldsymbol{\varepsilon}$ is the strain (6x1 vector) and $\boldsymbol{\sigma}$ is the stress (6x1 vector). Voigt notation is used to condense the tensor presentation from components 11, 22, 33, 23, 13, 12 into components 1, 2, 3, 4, 5, 6, respectively. $\mathbf{E}$ is the electric field (3x1 vector), $\mathbf{D}$ is the electric displacement (3x1 vector), $\mathbf{s}_F$ and $\mathbf{s}_D$ are compliance coefficients (6x6 matrix) at constant electric field and constant electric displacement, respectively. $\mathbf{c}_F$ and $\mathbf{c}_D$ are stiffness coefficients (6x6 matrix) at constant electric field and constant electric displacement, respectively. $\boldsymbol{\kappa}_\sigma$ and $\boldsymbol{\kappa}_\varepsilon$ are electric permittivity (3x3 matrix) at constant stress and constant strain, respectively. **d**, **e**, **g** and **h** are the piezoelectric coupling coefficients (3x6 matrix) relating the mechanical quantities ($\boldsymbol{\sigma}$ and $\boldsymbol{\varepsilon}$) to the electrical quantities ($\mathbf{E}$ and $\mathbf{D}$). The most commonly used piezoelectric coefficient is **d**, which for PVDF is generally reported as,

$$\mathbf{d} = \frac{\partial \mathbf{D}}{\partial \boldsymbol{\sigma}} = \begin{bmatrix} 0 & 0 & 0 & 0 & d_{15} & 0 \\ 0 & 0 & 0 & d_{24} & 0 & 0 \\ d_{31} & d_{32} & d_{33} & 0 & 0 & 0 \end{bmatrix} \tag{2}$$

Figure 4 illustrates the deformation of a piezoelectric material under different loading modes and the components of **d** that can be extracted from each mode. For each coefficient d_{ij}, subscript i is the direction of the polarization and subscript j is the direction of the applied force.

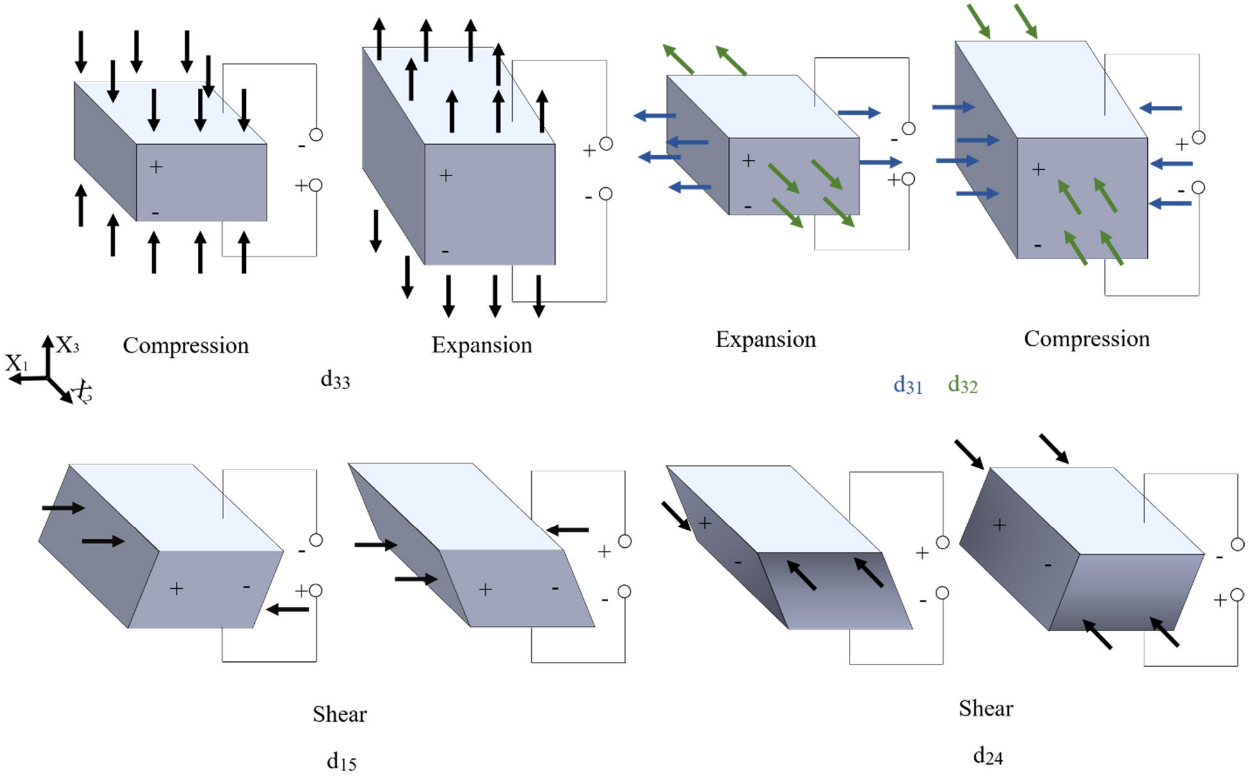

Figure 4. Deformation of piezoelectric material in different modes with corresponding piezoelectric coefficients and polarity of voltage output (+/- on material refers to polarization direction; +/- on circuit refers to polarity of output voltage).

3.2. Cyclic compression/impact test

Dynamic compression test and impact test are two of the most widely adopted characterization methods to measure the piezoelectric properties of electrospun PVDF fiber mats. When experiencing deformation under compressive load or impact in the direction perpendicular to the mat surface, the PVDF fiber mats generate a voltage under open circuit condition. For compression test, which is typically performed in a cyclic fashion, the force exerted on the PVDF fiber mats can be measured by a load cell. For impact test, the common method is dropping a known mass onto the sample from a given height. Instead of using a load cell, the following equation is used to estimate the impact force caused by a falling object [28],

$$F_{\text{falling object}} = \frac{m_{\text{object}}\sqrt{2gh}}{\Delta t} \tag{3}$$

where m_{object} is the mass of the falling object, g is the gravitational constant, h is the height from which the object is released, and Δt is the impact duration. This equation assumes that the mass completely stops after impacting the fiber mat and does not bounce back. Another type of impact test uses a pendulum. A known mass (m_{pendulum}) is tied to a string of prescribed length (l) and swung towards the PVDF sample. The average impact force generated by the pendulum can be calculated by [29],

$$F_{\text{pendulum}} = \frac{m_{\text{pendulum}}\left(\sqrt{2gl\left(1-\cos\theta_1\right)} + \sqrt{2gl\left(1-\cos\theta_2\right)}\right)}{\Delta t} \tag{4}$$

where θ_1 and θ_2 are the initial angle and the rebound angle of the pendulum.

Under the dynamic stress from compression or impact test, the dynamic piezoelectric coefficient d_{33} of the PVDF sample can be calculated from [30],

$$d_{33} = \frac{\int_0^t V\left(t\right)\mathrm{d}t}{AR\sigma_{\text{applied}}(t)} \tag{5}$$

where $V\left(t\right)$ is the output voltage at time t, $\sigma_{\text{applied}}(t)$ is the corresponding stress measured at time t, R is the test resistance, and A is the contact area of the PVDF sample the load is applied on. Eq. (5) is derived from Eq. (2), where the piezoelectric coefficient is calculated as partial derivative of electric displacement with respect to stress. $A\sigma_{\text{applied}}$ can be identified as the applied force, and the ratio between the obtained voltage and the measured force is defined as the sensitivity (in V/N). An alternative form of sensitivity has also been used, which is the ratio of the output voltage to the applied stress (in V/kPa). If the compression load is cyclic, the frequency of the compressive force can also affect the output voltage of the PVDF sample. Higher frequency can lead to higher voltage while causing more fluctuation in the output signal [31].

3.3. Bending test

An electrospun PVDF fiber mat can be subjected to bending deformation in order to measure its sensitivity (in V) as the ratio between the output voltage and the maximum strain in the sample. The common bending methods include cantilever beam [32], three-point bending [33], and buckling with simple support [34] or clamping [35] at the two ends of the sample. The open circuit output voltage is generally measured by oscilloscope [32–35], while the maximum strain estimated by the Euler-Bernoulli beam theory. Specifically, the PVDF sample is approximated by a uniform beam that obeys the assumptions in the Euler-Bernoulli beam theory [36]: (1) the cross section of the beam is uniform along the beam, and remains plane and perpendicular to the neutral axis; (2) the deflection is small; and (3) the beam is homogeneous, isotropic and linearly elastic.

Within the Euler-Bernoulli beam theory, the maximum strain for a cantilever beam is calculated by,

$$\varepsilon_{\text{cantilever, max}} = -\frac{M_{\text{cantilever, max}} h}{2EI} = \frac{3\Delta_{\text{cantilever, max}} h}{2L^2} \tag{6}$$

where E is elastic modulus, I is moment of inertia, L is the undeformed length of the beam, $\Delta_{\text{cantilever, max}}$ is the deflection at the end of the beam, $M_{\text{cantilever, max}}$ is the maximum bending moment which occurs at the clamped end, and h is the thickness of the beam. Under three-point bending, the maximum strain is

$$\varepsilon_{\text{three-point, max}} = \frac{6\Delta_{\text{three-point, max}} h}{L^2} \tag{7}$$

where $\Delta_{\text{three-point, max}}$ is the maximum deflection, occurring at the midpoint of the beam. For a buckled beam, the maximum strain is

$$\varepsilon_{\text{buckle-clamp, max}} = \frac{2\pi^2 \Delta_{\text{buckle-clamp, max}} h}{L^2} \tag{8}$$

if the two ends are clamped, and

$$\varepsilon_{\text{buckle-support, max}} = \frac{\pi^2 \Delta_{\text{buckle-support, max}} h}{2L^2} \tag{9}$$

if the two ends are simply supported. $\Delta_{\text{buckle-clamp, max}}$ and $\Delta_{\text{buckle-support, max}}$ are respectively the maximum deflections for the two cases, occurring at the midpoint of the beam. In the special situation where the radius of curvature ρ of the bent beam is constant, the maximum strain is the same along the beam and is given by,

$$\varepsilon_{\text{uniform, max}} = \frac{h}{2\rho} \tag{10}$$

which has been widely adopted for the bending of the electrospun PVDF-based fiber mats [37].

Some studies have moved away from the assumption of small deflection. Tiwari et al. approximated the effective bending strain for a buckled flexible sample with two ends clamped and a force (F_{applied}) applied in the center [38],

$$\varepsilon_{\text{three-point,clamp}} = 4\left(\frac{2}{\overline{F}}\right)^{\frac{1}{2}} \left\{ f\left[\sin^{-1}\left(n\sin\frac{\pi-\theta}{2}\right),\frac{1}{n}\right] - f\left[\sin^{-1}\left(\frac{n}{\sqrt{2}}\right),\frac{1}{n}\right]\right\} - 1 \qquad (11)$$

where $\overline{F} = F_{\text{applied}}L^2 / EI$ with limit of $\overline{F} < 64$ is a dimensionless force, $\cos\theta = \overline{F}/64$, $n = \sqrt{2/(1+\cos\theta)}$ and $f(\bullet)$ is the incomplete elliptical integral of the first kind. For a buckled film with simple supports. Persano et al. considered the bending of a fiber mat perfectly bonded to a substrate, and calculated the bending strain of the mat ($\varepsilon_{\text{buckle-support, energy}}$) using an energy approach [39],

$$\begin{aligned} \varepsilon_{\text{buckle-support, energy}} &= \frac{\pi^2 \Delta_{\text{buckle-support, max}} \left(h_{\text{substrate}} + h_{\text{piezo}}\right)}{L_{\text{substrate}}{}^2} \cos\left(\frac{2\pi X_3}{L_{\text{substrate}}}\right) \\ \Delta_{\text{buckle-support, max}} &\approx \frac{2}{\pi}\sqrt{L_{\text{substrate}}\Delta L} \end{aligned} \qquad (12)$$

As shown in Figure 5a, $h_{\text{substrate}}$ and $L_{\text{substrate}}$ are the thickness and the length of the substrate, h_{piezo} is the thickness of piezoelectric fiber mat, X_3 is the coordinate along the longitudinal direction of the fiber array, and ΔL is the reduced length of the substrate.

Besides strain, vertical or horizontal displacement [35], change in curvature, and bending angle [40,41] have been used as alternative indicators for the deformation of the bent sample. In addition, many studies have used numerical tools such as finite element to analyze the bending strain and piezoelectricity. Abbasipour et al. simulated the three-point bending of an electrospun PVDF fiber mat assuming it to be a solid film [33]. Even though the simulated deformation showed high resemblance to experimental data, the predicted voltage output deviated from experimental value. Alam et al. simulated the bending of an electrospun fiber mat induced by wind pressure [42]. The simulated higher output (2.3 V) than the experimental value (~1.8 V) was attributed to the charge dissipating between the piezoelectric layer and electrodes.

3.4. Vibration test

Vibration test is another method to induce deformation of the PVDF sample and generate voltage. While vibration can be produced from a wide range of sources such as wind flow, musical instrument, human speech, waterfall, etc. [43], lab-scale characterization is usually conducted by a vibration generator [44] or a speaker [43,45–47]. At higher decibel level, the acoustic pressure exerted on the PVDF sample is larger. Lee at al. reported that the output voltage of a PVDF sensor was linearly proportional to the decibel level of the sound exerted on the sensor [45]. Sound frequency is another important factor that affects the output voltage. The closer the sound frequency is to the resonance frequency of the PVDF sample, the larger is the vibration amplitude , inducing higher voltage output [47]. Since the sound produced by human, such as singing, humming, or coughing, has specific frequency, intensity, or profile, it can be distinguished using the near-field electrospun PVDF sensor [45].

Vibration-induced deformation can be used to quantify the piezoelectric response of electrospun PVDF fibers. Lim et al. characterized the tensile and compressive strains experienced by an electrospun PVDF fiber mat under vibration (Figure 5b) [48],

$$\begin{aligned} \varepsilon_{\text{tensile, bending}} &= \frac{L_{\text{outer}} - L_{\text{center}}}{L_{\text{center}}} \\ \varepsilon_{\text{compressive, bending}} &= \frac{L_{\text{inner}} - L_{\text{center}}}{L_{\text{center}}} \end{aligned} \tag{13}$$

where L_{outer} , L_{center} , L_{inner} are the lengths of the outer surface, neutral axis, and inner surface of the sample under bending as vibration is applied. The sensitivity reported in vibrational test is normally expressed as either output voltage per applied stress or output voltage per displacement [49]. Numerical simulation can also be used to obtain the oscillating deformation profile of energy harvesting devices based on electrospun PVDF [50].

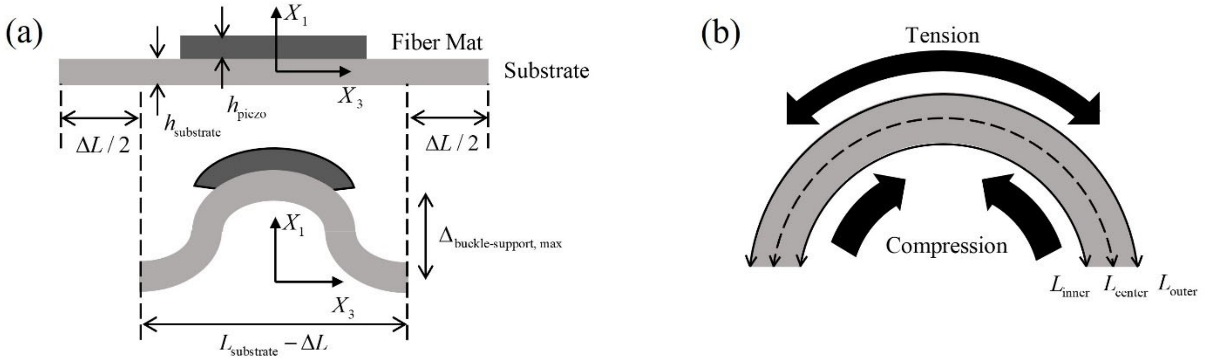

Figure 5. (a) Bending of fiber mat and substrate in [39] (b) Bending strain of piezoelectric fiber mat in [48]

3.5. Other tests

Other common testing methods to characterize the piezoelectric effect of PVDF samples include tensile test and torsion test [51,52]. Tensile test can be conducted on a single electrospun fiber or a fiber mat [52,53], although single-fiber tensile test is rarely used due to the difficulty to measure its small voltage output [52]. Tensile strain can be obtained from the change in the length of the fiber from its original (L) to elongated (L_{elongate}) values,

$$\varepsilon_{\text{tensile}} = \frac{L_{\text{elongate}} - L}{L} \tag{14}$$

Voltage/current output in response to an applied tensile strain is a commonly used piezoelectric characterization for the electrospun PVDF fibers [33,34,54,55].

Additional to the aforementioned characterizations, real-life mechanical stress, such as finger tapping, foot stepping, elbow bending and sound generating, can also be applied on the PVDF sample to characterize its piezoelectric response [35,56]. However, quantitative measurement of the applied force or deformation are sometimes not included for these human-contact tests. Standardization of such piezoelectric tests is recommended for future investigations.

4. Chemical Characterization

4.1. Fourier transform infrared spectroscopy (FTIR)

Characterization of the α, β, γ, and δ crystalline phases is generally conducted using FTIR. Absorption of infrared light by PVDF at different wavelengths is measured by FTIR to determine the functional groups and the crystalline phases. The commonly reported wavenumbers corresponding to the α phase of electrospun PVDF fibers are 482, 511, 610, 763, 976, and 1073 cm^{-1} [35,57]. The wavenumbers for the β phase are 472, 509, 841, 879, 1072, 1174, 1280, and 1402 cm^{-1} [35,55,57]. The wavenumbers for the α and β phases of PVDF pellets and membranes manufactured with other methods may deviate from those of electrospun PVDF fibers [58–60]. Addition of fillers and physical or chemical changes to PVDF may also cause the wavenumbers to shift. The wavenumbers for the β and γ phases share some similarities. The characteristic peak at 841 cm^{-1} is generally assigned to the β phase, but some researchers argue it is indistinguishable from the γ phase at the same wavenumber [59].

Under the assumption that absorption in the infrared spectrum complies with the Lambert-Beer law, the fraction of the *β* phase, or the *β* phase content, characterized with FTIR can be calculated by,

$$X_\beta = \frac{A_\beta}{\frac{K_\beta}{K_\alpha} A_\alpha + A_\beta} \tag{15}$$

where A_α is the absorbance at around 763 cm^{-1} corresponding to the *α* phase. A_β is the absorbance at around 841 cm^{-1} corresponding to the *β* phase. K_α and K_β are the absorption coefficients with values of $7.7 \mathrm{x} 10^4$ cm^2/mol and $6.1 \mathrm{x} 10^4$ cm^2/mol, respectively [58].

4.2. X-ray diffraction (XRD)

Another common method to characterize the crystalline phases of PVDF is XRD or wide-angle x-ray diffraction (WAXD), which irradiates x-rays onto the semicrystalline PVDF sample. The crystalline spacing can be identified from the scattered rays. The diffraction pattern at different angles shows characteristic peaks that can be assigned to specific crystal planes of each crystalline phase. For the electrospun PVDF fibers, peaks at 17.4°, 18.4-18.5°, 20.14-20.3°, 26.7° and 27.0° are normally assigned to the *α* phase with crystal planes of (100), (020), (110), (021) and (111), respectively [55,61–63]. Peaks at 20.1-20.8°, 31.9° or 36.6°, and 36.2° are typically assigned to the *β* phase with crystal planes of (200/110), (001) and (101), respectively [55,61–63]. Similar to wavenumbers in FTIR, assigning peaks to each crystalline phase is contentious.

The degree of crystallinity characterized from XRD can be calculated by [64],

$$X_c = \frac{\sum A_c}{\sum A_c + \sum A_a} \tag{16}$$

where $\sum A_c$ and $\sum A_a$ are respectively the summations of the areas under the peaks corresponding to crystalline and amorphous structures. To calculate the *β* phase content of the electrospun PVDF fibers from the XRD result [64],

$$X_\beta = \frac{X_c \sum A_\beta}{\sum A_\alpha + \sum A_\beta + \sum A_\gamma} \tag{17}$$

where $\sum A_\alpha$, $\sum A_\beta$, $\sum A_\gamma$ are respectively the summations of peak areas corresponding to *α*, *β* and *γ* phases assuming the crystalline structure is composed of these three phases. Area under the characteristic peak corresponding to (200/110) reflection of β phase can be used as the value of $\sum A_\beta$ [13].

4.3. Differential scanning calorimetry (DSC)

The crystallinity of electrospun PVDF fibers can be characterized using DSC. Upon the rise of temperature, the heat absorbed by a PVDF sample is dependent on the crystalline phases, defects, and crystalline size in the sample [59]. The degree of crystallinity can be calculated by [65,66],

$$X_c = \frac{\Delta H_f}{\Delta H_f^{\,o}} = \frac{\Delta H_f}{X_\alpha \Delta H_\alpha + X_\beta \Delta H_\beta} \tag{18}$$

where ΔH_f is the melting enthalpy of the electrospun PVDF fibers and $\Delta H_f^{\,o}$ = 104.7 J/g is the melting enthalpy of PVDF with 100% crystallinity [65]. ΔH_α (93.07 J/g) and ΔH_β (103.4 J/g) are the melting enthalpies for 100% crystalline α and β phases, respectively [66]. X_α is the α phase content and X_β is the β phase content, which can be obtained from the previously described characterization methods.

The results from FTIR, XRD, and DSC can be combined to describe the crystalline structures in electrospun PVDF fibers. Even though the fraction of β phase, X_β, is the general indication of the β phase content, the actual β phase content in the sample is dependent on both X_β and the degree of crystallinity [64]. The combination of these characterizations provides a good estimation and cross-validation for the β phase content.

5. Effect of Electrospinning Parameters on Piezoelectric Output

5.1. Electric field

In the solution electrospinning process, the strength of the electric field exerted on the discharged PVDF solution is the ratio between the applied voltage and the tip-to-collector distance. The electric field strength determines the elongational stress experienced by the jet extruded from the spinneret. At higher electric field, the jet is stretched into fiber with smaller diameter. Mechanistically, at a given tip-to-collector distance, if the applied voltage is increased, the charge density over the jet surface increases which leads to higher reduction in jet diameter and higher acceleration of the jet. Insufficient voltage results in either failure to form the Taylor cone or unstable Taylor cone with solution dripping at the tip. On the other hand, if the voltage increases beyond a certain limit, the high surface charge exerts excessive stress on the jet and causes the jet to break off. The electric field can also be increased by decreasing the tip-to-collector distance. A sufficient tip-to-collector distance is required for the solvent to fully evaporate before reaching the collector. If the PVDF jet is not solidified, the collected fibers can exhibit defects, such as ribbon-like fibers, unsmoothed surfaces, beads, or electrospraying [67]. Increasing the tip-to-collector distance can lengthen the traveling time to reduce the diameter of the fiber, at the expense of weakening the electric field. On that account, different effects of the tip-to-collector distance on the fiber diameter have been reported [68,69].

There has been some debate about the effect of the electric field on the β phase content and degree of crystallinity. Intuitively, when increasing the electric field, the molecular chains of the PVDF jet are more oriented along the jet direction so that higher degree of crystallinity can be expected after solidification. The work of Jin et al. is consistent with this speculation, where increasing the tip-to-collector distance, hence reducing the electric field, lowered the degree of crystallinity [64]. On the other hand, the change in the tip-to-collector distance had no effect on the β phase content [64]. A completely different trend was reported by Gee et al., who discovered that the β phase content increased from 70.9% to 83.5% as the tip-to-collector distance changed from 10 cm to 16 cm [70]. Similarly, Ribeiro et al. reported that increasing the applied voltage from 15 kV to 30 kV caused the β phase content to reduce from 86% to ~81% [66], while the degree of crystallinity did not show significant change. The authors attributed the decrease in the β phase content to the applied voltage exceeding the limit, which induced jet instability and posed negative effect on the formation of electroactive β phase. Jiyong et al. reported that the β phase content increased from ~70% to ~76% as the applied voltage increased from 14 kV to 20 kV [71]. Further increase caused the β phase content to reduce (~71% at 24 kV). The degree of crystallinity followed the same trend, which increased from ~48% at 14 kV to ~58% at 20 kV and reduced to ~52% at 24 kV. This work suggests that an optimal electric field may exist that maximizes the β phase content and degree of crystallinity. Shao et al. reported that the tip-to-collector distance had a positive correlation with the β phase content when the distance was smaller than 2 cm and a negative correlation with the degree of crystallinity at distance smaller than 6 cm [69]. They also found that the PVDF solution only formed fibers at specific combinations of applied voltage and tip-to-collector distance. The interactive effect between the applied voltage, tip-to-collector distance and other parameters, such as flow rate and solution properties, should be investigated when optimizing the electrospinning process. It is recommended to first find the range of distance for which uniform fibers can be produced and then adjust the applied voltage to modulate the electric field exerted on the PVDF solution.

5.2. Flow rate and needle diameter

Flow rate is one of the most significant factors that can influence the morphology, *β* phase content, and degree of crystallinity of electrospun PVDF fibers [68]. It controls the mass of the PVDF solution fed into the electrospinning process. At higher flow rate, higher electric field is required to achieve sufficient stretching and poling of the jet. Otherwise, the alignment of the molecular chain in the jet direction reduces and the *β* phase content may decrease. Several works have reported negative correlation of the *β* phase content and degree of crystallinity with the flow rate [68,71]. It should be noted, however, very low flow rate can lead to discontinuous jet formation especially at high electric field. Gee et al. did not find any correlation between the flow rate and the *β* phase content when the flow rate was lower than 0.8 ml/hr [70]. Jiyong et al. also stated that the reduction of the degree of crystallinity with the flow rate was only observed for flow rate higher than 1 ml/hr [72]. Thus, it is crucial to find the appropriate range of flow rate for maintaining uniform jet in electrospinning.

Similar to the flow rate, increasing the needle diameter also increases the mass of the jet and results in larger fiber diameter. Ribeiro et al. discovered that the *β* phase content decreased from 86% to 53% when the needle diameter increased from 0.25 mm to 0.50 mm [66]. If a smaller needle diameter is chosen to yield smaller fiber diameter, the flow rate should be adjusted to avoid discontinuous jet formation, else the piezoelectric properties of the produced PVDF fibers may be impacted. Other than the diameter, the length of the needle also poses an impact on the fiber diameter and the polymer crystallinity. Tian et al. found that as the length of the needle increased, the fiber diameter decreased with increasing polymer crystallinity [73]. The saturation of the change in crystallinity occurred after the needle was long enough for the polymer solution to achieve fully developed flow. Therefore, the rheology of the polymer flow affected by the geometry of the needle is crucial to tailor the properties of the PVDF fibers.

5.3. Apparatus configuration

The collectors in the electrospinning process can be customized to achieve different configurations of the PVDF fibers. To yield random fibers, a flat plate or a collector rotating at a low speed can be used. To produce aligned fiber arrays, rotating drum [66], rotating ring [74], centrifugal electrospinning [75], gap electrospinning [76], etc. can be adopted. For more control over the fiber layout, direct-writing or near-field solution electrospinning can tailor the direction and alignment of the electrospun PVDF fibers [54]. Aligned fibers are expected to show better piezoelectric properties due to more oriented dipole distribution over the surface of the fiber mat. Using a rotating collector can assist in obtaining better molecular chain orientation in the fiber direction since centrifugal force tangential to the rotating drum rotation can apply extra stretching. Rotating drum is one of the most widely reported methods to produce aligned electrospun PVDF fibers, on account of its ease of operation. Singh et al. showed that increasing the drum rotating speed from 500 rpm to 750 rpm increased the β phase content from 75% to 81.3%, but further increase in the rotating speed caused the β phase content to decrease [65]. This reduction after reaching a threshold rotating speed was ascribed to interruption of the fiber stretching induced by the air flow arising from high rotation. The positive correlation between β phase content and the rotating speed at low speed and the presence of an optimal value were also reported in other works [66,68].

The electrospun PVDF fibers are not limited to a solid cylindrical shape. Hollow fibers and core-shell composite fibers have also been reported by adopting different spinnerets. Sharafkhani and Kokabi fabricated electrospun PVDF fibers with several different structures and properties (β phase content, degree of crystallinity): random solid fibers (72%, 34.2%), aligned solid fibers (79%, 36%), random hollow fibers (86%, 39.5%), and aligned hollow fibers (90%, 44%) [77]. In comparison to solid fibers, hollow fibers possess higher specific surface area. Confining the molecular chains within the shell structure of hollow fibers promotes more oriented crystal growth in the fiber direction. Generation of hollow fibers also makes it feasible to incorporate piezoelectric ceramics, which has better piezoelectric properties, as the core. Investigating production of electrospun PVDF fibers with such structures is of interest in the development of flexible smart textiles with enhanced piezoelectric properties.

To form smart textiles, post-processing electrospun PVDF fiber mat into yarns by braiding or spinning is not ideal since it generates extra production cost. Some novel electrospinning apparatuses have been proposed to directly produce electrospun PVDF yarn from the solution. The yarn can be drawn from a cone, a ring, or a water bath, which assembles the individual fibers into a yarn by twisting or stretching [74,78,79]. Peng et al. used a rotating cone with a hole, which fed a conductive core for yarn to be wrapped on, and two spinnerets polarized with opposite voltage to produce PVDF composite yarns [79]. The PVDF fibers were wrapped around the core, and the degree of wrapping was quantified by a parameter called twist per meter defined as the ratio of the twisting speed over the translational speed at which the yarns were collected. The β phase content and the degree of crystallinity showed a positive relationship with twist per meter up to an optimal value. However, their reported β phase content (~36%) was poor compared to other works. Gao et al. formed PVDF yarns with a similar structure and reported β phase content of 79.5% [80]. Even though this β phase content is comparable to the value for other structures, further research needs to be done to fully understand if yarn electrospinning can enhance the piezoelectric properties of PVDF fibers.

Polarity is a parameter that can be easily overlooked since applying positive charge on the spinneret and grounding the collector is the most common setup used in electrospinning of PVDF fibers. Szewczyk et al. demonstrated that reversing the polarity on the spinneret from negative to positive while grounding the collector caused a minor change in the degree of crystallinity, a slight enhancement in the β phase content (from 17.8% to 18.3% measured by DSC) and a better piezoelectric response (from 2.565 to 5.558 pm/V measured by piezoresponse force microscopy) [13]. They reported that positive polarity attracted more negative fluorine element on the surface: the fluorine/carbon ratio increased from 0.78 to 0.89 when the polarity changed from negative to positive. Therefore, polarity can play a role in modifying surface chemistry and improving piezoelectric properties of electrospun PVDF fibers.

5.4. Relative humidity and ambient temperature

Environmental parameters have substantial impact on solvent evaporation during electrospinning. The two predominant factors are relative humidity and ambient temperature. If the environment is humid, the evaporation rate of the volatile solvent is suppressed and the surface charge distribution is affected. At short distance, slower evaporation rate can cause incomplete solvent evaporation. At long distance, slower evaporation rate can induce further reduction in jet diameter due to longer duration for deformation by electric field. A systematic study was conducted by Zaarour et al. to understand how to control the morphology of the electrospun PVDF fibers [67]. As the relative humidity increased, the produced fibers changed from uniform solid fibers into unsmooth fibers with interior and surface pores, or a grooved surface. Formation of surface pores was attributed to thermal-induced phase separation, where the temperature decreased due to solvent evaporation. Formation of interior pores was attributed to vapor-induced separation, where water condensed on the extruded PVDF jet, penetrated the boundary, and led to pore formation during evaporation. Formation of grooved fibers was attributed to the trapped solvent inside the solidified skin; evaporation of the trapped solvent induced surface collapsing towards the interior. In a separate work, Zaarour et al. discovered that increasing the relative humidity from 2% to 62% caused the β phase content and the degree of crystallinity to increase from 55% to 73.06% and from 44.17% to 57.32%, respectively [81]. Longer evaporation time at higher humidity promoted molecular chain alignment and β phase formation. In general, low relative humidity is favored in order to form uniform PVDF fibers with stronger mechanical properties, while potentially sacrificing the β phase content and the degree of crystallinity. Relative humidity is hence a factor that can be used to tailor the morphology and piezoelectric properties of electrospun PVDF fibers for different applications.

The viscosity of the PVDF solution is higher at lower temperature, requiring higher electric field to overcome the surface tension and form a jet. On the other hand, increasing the temperature can increase the evaporation rate of the solvent, leading to faster solidification and thicker fibers. Huang et al. observed that an optimal temperature existed for electrospinning PVDF solution, because the degree of crystallinity increased from 38.5% at 15°C to 52.9% at 25°C and decreased to 44.8% at 45°C [82]. They considered the initial increase to be caused by lowered surface tension and enhanced stretching as the temperature increased. Further increment caused shorter evaporation time and thus reduced degree of crystallinity. Overall, the ambient environment has considerable effect on the piezoelectric properties of electrospun PVDF fibers.

5.5. Solution properties

Solution properties impact the rheology of the solution and subsequently the behavior of the jet. The main solution properties include molecular weight of PVDF, selection of solvent, solvent ratio, and PVDF concentration. Molecular weight is related to polymer entanglement in the solution [66]. Higher molecular weight increases the viscosity of the PVDF solution and produces fibers with larger diameter. Zaarour et al. increased the molecular weight of PVDF from 180 kDa to 530 kDa to produce aligned electrospun fibers, which led to improvement in the β phase content from 80.33% to 88.64%, increase in the degree of crystallinity from 48% to 55%, and higher output voltage from ~1.97 V to ~2.92 V under the same compressive force of 10N and frequency of 5 Hz [83]. They believed that the improvement in the piezoelectric properties was achieved by longer evaporation time associated with higher viscosity, which helped achieve better stretched molecular chains. However, the produced fibers were grooved and interior pores were present. Increasing molecular weight over a certain limit can decrease the specific area of the fibers due to larger diameter, increase the surface tension of the solution, and make the electrospinning process challenging.

PVDF is soluble in various dipolar aprotic solvents, and the selection of the solvent has a strong influence on the electrospinning behavior of the PVDF jet and the piezoelectric properties of the produced fibers. Unlike membrane fabrication methods where evaporation rate is the main parameter to consider, the solubility of PVDF in the solvent, as well as the dielectric properties and vapor pressure of the solvent all play crucial roles. To determine the solubility of PVDF, Hansen solubility parameter (HSP) is generally used. The Hansen coordinate space consists of three axes, SP_d, SP_p, and SP_h, corresponding to dispersion, polar, and hydrogen-bonding solubility parameters, respectively. The solubility of a solute in a solvent is evaluated as the distance from a point in the Hansen space that represents the solvent to a point that represents the solute [84],

$$R_a = \sqrt{4\left(SP_{d,\,\text{solvent}} - SP_{d,\,\text{solute}}\right)^2 + \left(SP_{p,\,\text{solvent}} - SP_{p,\,\text{solute}}\right)^2 + \left(SP_{h,\,\text{solvent}} - SP_{h,\,\text{solute}}\right)^2} \tag{19}$$

A reference distance, R_o, is obtained from experiments to gauge the solubility of PVDF, through the so-called relative energy difference (RED) [84],

$$\text{RED} = \frac{R_a}{R_o} \tag{20}$$

If RED is smaller than 1, the solvent is good; otherwise the solvent is not suitable for dissolving PVDF. The dielectric constant of the solvent determines the charges required to polarize the solution into thin jet. Solvent with a high dielectric constant makes elongation of the solution under the electric field easier, due to higher amount of free charges available on the surface. However, excessive free charges may cause instability, promoting the formation of beads. Vapor pressure is related to the evaporation rate of the solvent. At room temperature, solvent with a low vapor pressure is less volatile and evaporates more slowly. This prolongs the stretching process to yield thinner fibers. However, in near-field electrospinning, lower evaporation rate may cause incomplete solvent evaporation and induce fusion. Viscosity and surface tension of the solvent also affect the electrospinning behavior. Common solvents used for electrospinning PVDF are listed in Table 1, along with their properties.

The most commonly used solvents for PVDF are DMF, acetone, or their various level mixtures. Gee et al. examined three binary solvents, DMF/acetone, DMSO/acetone, and NMP/acetone (6/4 v/v), which produced electrospun PVDF fibers with β phase content of 90.9%, 87.4%, and 81.9%, respectively [70]. The fibers were finer and smoother with more uniform diameter distribution when DMF/acetone was used. The authors attributed the poorer properties yielded with DMSO and NMP to their higher surface tension and viscosity. It was further found that for the DMF/acetone mixture, the β phase content decreased with DMF fraction. Cozza et al. also reported that higher DMF fraction led to reduction in β phase content and formation of beads [85]. It was believed that the lower vapor pressure of DMF limited solvent evaporation and the residual solvent caused undesired morphology. However, increasing the acetone fraction over a certain limit affected the interaction between PVDF chains and the binary solvent since PVDF had lower solubility in acetone. The widely used weight ratio or volume ratio between DMF and acetone is 2/3 or 3/2 [33,35,40,86].

Another critical solution property is the concentration of PVDF. Increasing PVDF concentration in the solution increases the overall viscosity and surface tension. Costa et al. demonstrated that increasing PVDF concentration in DMF/acetone mixture from 5 wt% to 10 wt% increased the degree of crystallinity from 45.2% to 53.1% [87]. Saha et al. confirmed the trend by showing that increasing PVDF concentration from 10 wt% to 12 wt% produced higher piezoelectric sensitivity from 140 mV/kPa to 160 mV/kPa, but further increment to 15 wt% caused the sensitivity to reduce to 126.67 mV/kPa [88]. This suggests increasing PVDF concentration in the solution up to an optimal value can improve the piezoelectric properties of electrospun PVDF fibers.

Table 1. Common solvents for PVDF reported in literatures and their properties [84,89,90]

Material	Hansen Solubility Parameters				Vapor Pressure at 21°C (mmHg)	Dielectric Constant at 20°C	Surface Tension at 20°C (dyn/cm)	Absolute viscosity at 25°C (cP)
	SP_d	SP_p	SP_h	RED				
Acetone	15.5	10.4	7.0	1.1	194	20.6	23.3	0.33
DMAc	16.8	11.5	10.2	0.3	1.0	37.8	34	0.92
DMF	17.4	13.7	11.3	0.3	3.8	36.7	35	0.82
DMSO	18.4	16.4	10.2	0.9	0.7	46.6	43.7	2.0

NMP	18.0	12.3	7.2	0.8	0.3	32.2	40.7	1.8
PVDF	17.1	12.6	10.6	$R_0 = 5.0$	-	-	-	-

6. Effect of Nanofillers and Additives

Piezoelectric properties of electrospun PVDF fibers can be tailored by addition of fillers. To achieve enhanced piezoelectric performance, fillers can either possess better piezoelectric responses than PVDF, induce formation of PVDF electroactive phases, or improve electron charge transfer in PVDF. The β phase nucleation can be promoted by hydrogen bond formation, ion (charge)-dipole interaction, radical reaction, etc. Figure 6 summarizes the fillers that have been discussed in recent works to improve the piezoelectric properties of electrospun PVDF fibers. These fillers can be subcategorized into seven main groups: piezoelectric ceramics, salts, carbon-based or conductive fillers, noble metal, natural biodegradable fillers, hydrophilic fillers, and clay. In this section, the output voltages of the electrospun PVDF fibers with addition of various fillers at different loading conditions were compared. If the loading condition was not reported in the review, it was owing to lack of description in the original works.

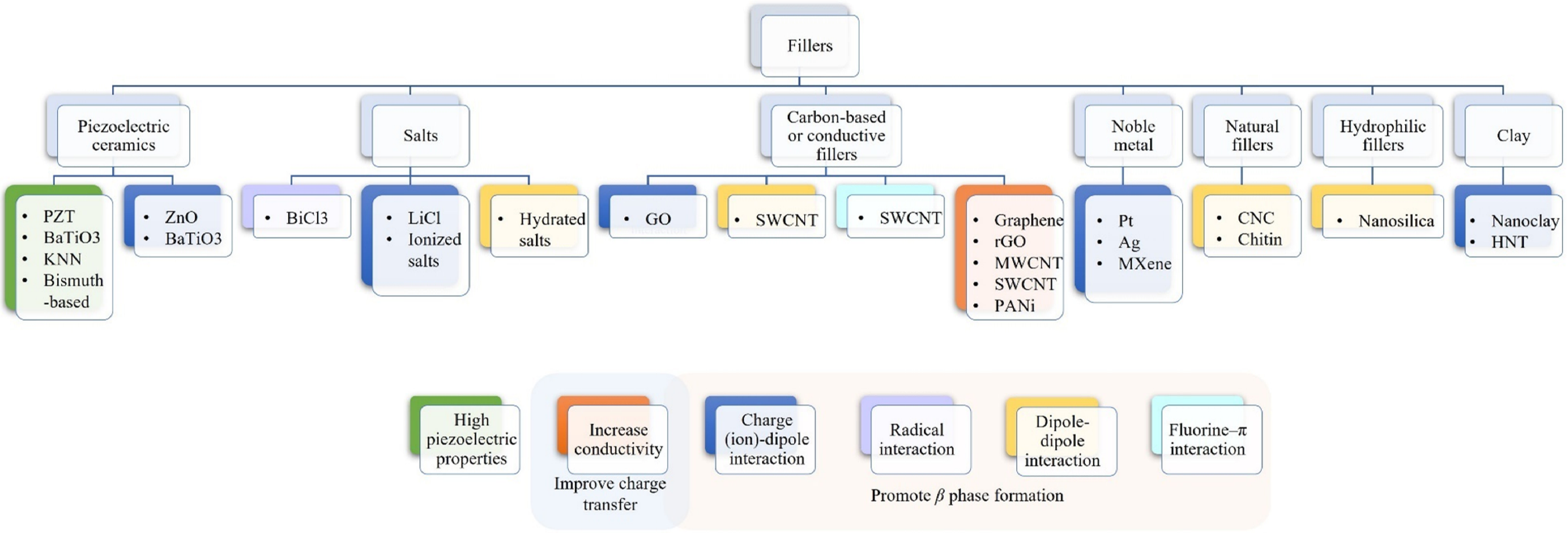
Fillers
Piezoelectric ceramics
PZT
BaTiO3
KNN
Bismuth -based
ZnO
BaTiO3
Salts
BiCl3
LiCl
Ionized salts
Hydrated salts
Carbon-based or conductive fillers
GO
SWCNT
SWCNT
Graphene
rGO
MWCNT
SWCNT
PANi
Noble metal
Pt
Ag
MXene
Natural fillers
CNC
Chitin
Hydrophilic fillers
Nanosilica
Clay
Nanoclay
HNT
High piezoelectric properties
Increase conductivity
Improve charge transfer
Charge (ion)-dipole interaction
Radical interaction
Dipole-dipole interaction
Fluorine–π interaction
Promote β phase formation

Figure 6. Summary of piezoelectric fillers and their mechanisms to improve the piezoelectric properties of the electrospun PVDF fibers (bottom row shows color scheme for fillers).

6.1. Piezoelectric ceramics

The most widely adopted filler is piezoelectric ceramics, which can be categorized into two main groups: lead-containing and lead-free ceramics. Examples of lead-containing ceramics include PZT and PZT-Lead Titanate (PZN-PT). Lead-free piezoelectric ceramics include three main perovskite families, Barium Titanate ($BaTiO_3$)-based, alkaline niobates-based, and bismuth-based perovskites [91,92]. For instance, the d_{33} values of PZT, PZN-PT, $BaTiO_3$, and sodium potassium niobate (KNN) are 225-374 pC/N, 2500 pC/N, 191 pC/N, and 160 pC/N, respectively [93–95]. Considering the much lower d_{33} value of PVDF (16.8-27.4 pC/N) [40], integrating piezoelectric ceramics into the electrospun PVDF fibers can improve the piezoelectric properties. For instance, PZT, one of the ceramic materials with high piezoelectric coefficients and dielectric constant, has been demonstrated in several works to improve the piezoelectric performance of electrospun PVDF fibers. Chamankar et al. used PZT with d_{33} value of 104 pC/N and concentration of 37 vol% (60 wt%) as a filler to obtain electrospun PVDF/PZT composite fibers that had β phase content of 70%, d_{33} value of 22.93 pC/N, and output voltage of 184 mV under applied force of 2.125 N [96]. The PZT particles behaved like dipole moments, contributing to local electric field and affecting the PVDF chain orientation. Koç et al. employed a type of PZT with substantially high d_{33} value (630 pC/N) to further improve the piezoelectric properties of aligned electrospun PVDF fibers [97]. The produced composite fibers with 10 vol% PZT exhibited highest output voltage of 440 mV under vibration frequency of 15 Hz. Higher PZT concentration reduced the piezoelectric response due to particle agglomeration. Lately, Du et al. managed to fabricate a high-performance PVDF/PZT device from hot-pressed multi-layered aligned electrospun PVDF/PZT fibers, which produced maximum output voltage of 62 V under cyclic compression of 5 N [98]. Even though PZT can considerably enhance the piezoelectric properties of electrospun PVDF fibers, the toxic lead content limits the application of such filler. Alternative lead-free ceramics that can achieve similar piezoelectric performance have attracted more research interests in recent publications.

$BaTiO_3$, the first piezoelectric ceramics fabricated in history, is one of the most extensively investigated lead-free substitutions of PZT. Guo et al. manufactured a pressure sensor from electrospun PVDF composite fibers with 3 wt% $BaTiO_3$ nanowire (NW) [99]. The composite fibers exhibited voltage sensitivity of 0.017 V/kPa with output voltage increasing linearly with the applied pressure until saturation at 40 kPa. Higher concentration of $BaTiO_3$ (20-25%) was analyzed by Hussein et al. [63] Although the highest β phase content was observed for fibers prepared from the solution containing 14% PVDF and 20% $BaTiO_3$, under an applied force of ~32 N, the highest output voltage of ~6.5 V was obtained for fibers prepared from 20% PVDF and 25% $BaTiO_3$ solution. This voltage was more than twice the output from fibers produced from pure PVDF. Higher piezoelectric response of electrospun PVDF/$BaTiO_3$ fibers was reported by Jiang et al. [46]. It was found that by increasing the concentration of $BaTiO_3$ from 0 wt% to 10 wt%, the β phase content of the composite fibers increased from 85.6% to 91% with the degree of crystallinity increasing from 37.4% to 42.3% and output voltage from ~20 V to ~50 V (Figure 7a). Further increment in $BaTiO_3$ to 20 wt% reduced the β phase content due to aggregation. A high voltage sensitivity of 18 V/N (Figure 7b) was achieved for a flexible device (Figure 7c) fabricated from electrospun PVDF fibers with 10 wt% $BaTiO_3$ under compressive loading. The authors attributed the improvement of the β phase content to suppressed chain relaxation of PVDF in the presence of $BaTiO_3$, as well as interaction between the negatively charged $BaTiO_3$ and the dipoles of PVDF which promoted β phase nucleation. The feasibility of using the PVDF/$BaTiO_3$ device for voltage generation from human motion such as finger bending was demonstrated (Figure 7d-e).

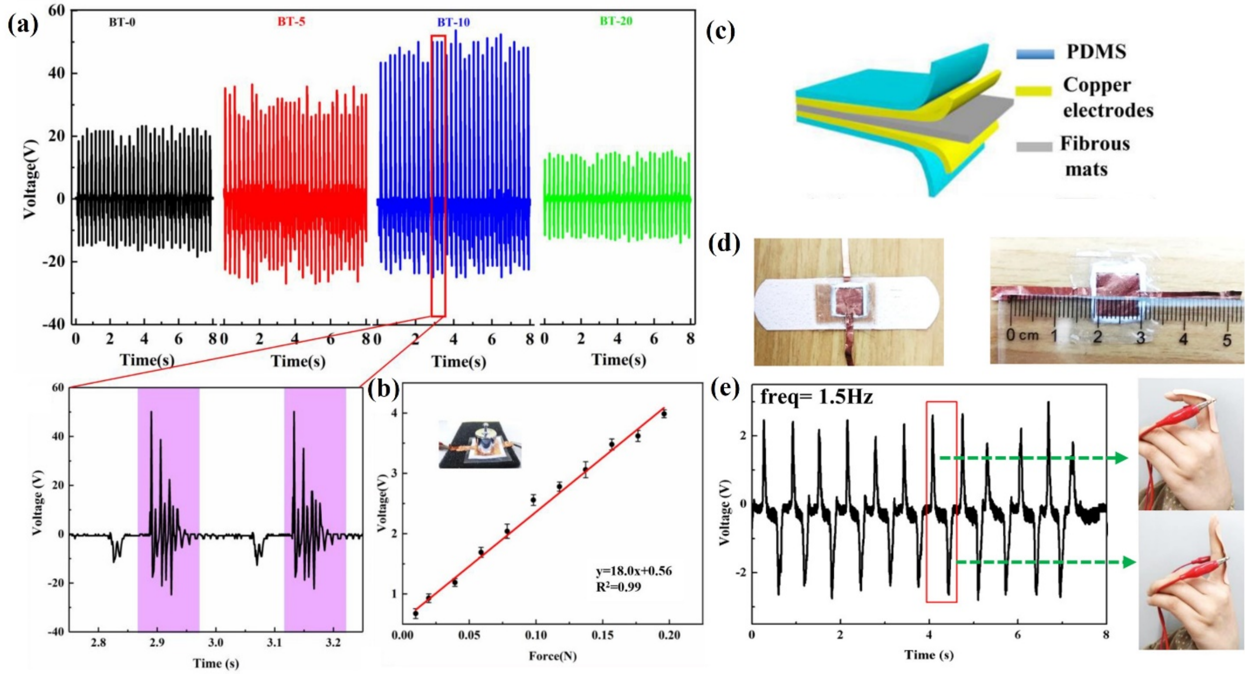

Figure 7. (a) Output voltages of electrospun PVDF fibers with 0-20 wt% BaTiO3, (b) voltage vs. force plot with slope being the voltage sensitivity, (c) device produced from electrospun PVDF

fibers with 10 wt% BaTiO3, (d) dimension of the device prepared for finger bending test, (e) output voltage generated from finger bending. Reprinted (adapted) with permission from Jiang et al., Flexible Piezoelectric Pressure Tactile Sensor Based on Electrospun BaTiO3/Poly(vinylidene fluoride) Nanocomposite Membrane, ACS Appl Mater Interfaces, 12,33989–98, Copyright 2020 American Chemical Society.

KNN, an alkaline niobate with piezoelectric coefficients comparable to PZT, has also been studied as a filler for electrospun PVDF fibers. Teka et al. demonstrated that including 5 wt% KNN in the electrospun PVDF fibers increased the β phase content from 64% to 68% and the output voltage from 0.05-0.1 V to 1.9 V measured by finger tapping [100]. Disparate observation was reported by Bairagi and Ali, concluding that KNN loading posed negative impact on β phase crystallization [101]. In their studies, the β phase contents of the electrospun PVDF fibers were 97%, 78%, and 84% at KNN concentration of 0%, 3%, and 5%, respectively. However, under the applied load of 0.5 N and frequency of 10 Hz, the highest voltage output of 17.5 V was obtained at 3% KNN, compared with 0.5 V from pure PVDF electrospun fibers. Therefore, KNN was considered to improve the piezoelectric properties of the electrospun PVDF fibers due to its higher piezoelectric coefficient, instead of promoting β phase formation.

Examples of bismuth-based piezoelectric ceramics include Sodium Bismuth Titanate [102], Bismuth Ferrite (BFO) [103], Bismuth Neodymium Titanate [104], etc. These materials possess good piezoelectric properties but limited work has been done to employ bismuth-based fillers in electrospun PVDF composite fibers. This is an intriguing research direction in the development of high-performance electronic textiles.

Beside perovskites, Zinc Oxide (ZnO) is a semiconducting ceramic that shows piezoelectric effect in a unique hexagonal wurtzite structure [105]. Considerable research has been conducted to incorporate ZnO as a filler for electrospun PVDF fibers. Bafqi et al. demonstrated that by increasing ZnO content from 0 wt% to 15 wt%, the β phase content increased from 80% to 87%, the degree of crystallinity increased from 51.4% to 54.5%, and the output voltage increased from 0.315 V to 1.1 V [106]. Ma et al. subsequently produced electrospun PVDF composite fibers by including 10 wt% ZnO NW using two parallel electrodes. The β phase content was improved and the output voltage increased from 0.143 V to 0.48 V under cantilever beam bending at a frequency of 10 Hz [107]. The increase in the β phase content was potentially caused either by ZnO affecting the stretching of PVDF chains during electrospinning, or by ZnO serving as a semiconductor generating local electric field to interact with PVDF chains. At low concentration of 0-0.1 wt%, Satthiyaraju and Ramesh reported that the *β* phase content of the electrospun PVDF fibers increased with ZnO concentration from 55.29% to 74.24% [108]. The highest d_{33} value (13.42 pC/N) was obtained at 0.1 wt% ZnO, compared with 8.29 pC/N for pure PVDF fibers. Li et al. further compared two forms of ZnO, ZnO nanoparticle (NP) and ZnO nanorod (NR) [109]. At the optimal concentrations, 30 wt% for ZnO NP and 5 wt% for ZnO NR, the electrospun PVDF/ZnO composite fibers exhibited *β* phase content of 87.5% and 90.7%, respectively. The higher *β* phase content obtained with ZnO NR was attributed to its higher aspect ratio, which had negatively charged surface interacting with the $-CH_2$ dipoles of PVDF to nucleate *β* crystallites. When subjected to bending under the frequency of ~4 Hz, the maximum output voltage of ~85 V was achieved with ZnO NR filler, and the associated degree of crystallinity was reported to be ~53.1%. More recently, Fu et al. converted the electrospun PVDF/Zinc Acetate fibers into PVDF/ZnO fibers via hydrothermal reaction [110]. Even though the *β* phase content did not change significantly, the maximum voltage output (0.352 V) was 2.74 times higher than the output of the pristine PVDF fibers.

Piezoelectric ceramics are among the most effective fillers that improve the piezoelectric properties of electrospun PVDF fibers. Some challenges still exist for using piezoelectric ceramics as fillers. For example, high concentration of piezoelectric ceramics induce aggregation and reduce flexibility, and some ceramics exhibit negative effect on promoting *β* phase formation. Further work can be conducted to facilitate uniform dispersion of high ceramic loading in the electrospun PVDF fibers without sacrificing ductility, increase interaction between the fillers and the PVDF chains by surface modifications, and fabricate piezoelectric ceramics with high aspect ratio to yield higher piezoelectric performance.

6.2. Salts

The mechanisms by which salt fillers improve *β* phase formation can be divided into three major categories: ion interaction [55], hydration [32], and dipole moment [111]. Some ionized salts can react with the radicals of PVDF to induce *β* phase formation while others can orient the PVDF chains by ion-dipole interactions. Hydrated salts with hydroxyl groups can form hydrogen bond with the fluorine atoms of PVDF to cause nucleation of the *β* phase. The dipole moments of polar salt fillers can interact with the $-CF_2$ or $-CH_2$ dipoles in PVDF to promote *β* phase crystallization.

Bismuth Chloride ($BiCl_3$) is a representative salt that can bind with the radicals of PVDF. Chen et al. added 1-10 wt% $BiCl_3$ to produce electrospun PVDF/$BiCl_3$ composite fibers. It was discovered that the fiber diameter decreased with filler concentration due to improved conductivity until 4 wt% after which increased solution viscosity counteracted the higher charge density [55]. As the filler concentration increased from 0 wt% to 7 wt%, the β phase content of the composite fibers increased from 75.2% to 85.7% and the degree of crystallinity from 37.5% to 39.5%, but further increase in filler concentration showed negative effect on β phase formation. The β phase enhancement was induced by Bi^{3+} and Cl^- ions in the solution which reacted with the charged radicals of PVDF, affecting the structure around the crystal lattices and causing the free radicals of PVDF to reposition into β crystallites. Impact tests were performed by dropping a 14.0 g ball from a height of 9 cm onto the electrospun fibers, and the maximum output voltage (38 V) was obtained from fibers loaded with 2 wt% $BiCl_3$. Zhang et al. confirmed the enhanced piezoelectric performance of the electrospun PVDF composite fibers with 2 wt% $BiCl_3$, as the β phase content increased from 76% to 84% and the d_{33} value increased from 1.74 pC/N to 2.14 pC/N compared with pure PVDF fibers [112]. Another ionizable salt is Lithium Chloride (LiCl) which has been reported to interact with the dipoles of PVDF in ionized form. Mokhtari et al. reported the production of electrospun PVDF composite fibers with 0-0.004 wt% LiCl [113]. At 0.00133 wt% LiCl, the highest β phase content (94.3%) was achieved, compared with 84% for pure PVDF fibers. Additionally, the fiber diameter decreased from 340 nm to 65 nm due to increased conductivity. LiCl concentration above 0.00133 wt% led to beads and reduced β phase content. In their subsequent work, impact tests were performed by dropping a steel ball with mass of 12 g from a height of 20 cm onto the samples [114]. Electrospun PVDF/LiCl composite fibers at the optimal concentration (0.00133 wt% LiCl) produced an output voltage of 5 V, much higher than the 1.3 V output voltage from pure PVDF electrospun fibers. The enhancement was attributed to the ion-dipole interaction between the dissociated ions of LiCl in the solvent and the dipoles of PVDF. These results demonstrate the feasibility of using ionized salts to improve piezoelectric properties of electrospun PVDF fibers at low concentration, while high concentration of ionized salt can disturb production of uniform ultrafine fibers by affecting the conductivity and the viscosity of the solution.

For the hydrated salts, water molecules are loosely bound to the salt crystals to facilitate hydration. The functional groups on the surface can interact with the dipole moments of PVDF to form β phase crystallites. Dhakras et al. examined Nickel Chloride Hexahydrate ($NiCl_2 \cdot 6H_2O$) and reported highest output voltage of 0.762 V at the optimal filler concentration of 0.5 wt%, when the sample was subjected to cantilever deformation with a maximum strain of 950 με [32]. In comparison, the output voltage was 0.296 V for pure PVDF electrospun fibers. Hydrogen bond formation between water attached to $NiCl_2$ and the dipoles of PVDF gave rise to β phase nucleation, inducing improvement of the piezoelectric response. Another hydrated salt, Aluminum Nitrate Nonahydrate ($Al(NO_3)_3 \cdot 9H_2O$) with concentration of 8-16 wt% was investigated by Yousry et al. [115]. After adding 8 wt% $Al(NO_3)_3 \cdot 9H_2O$, the fiber morphology changed from beaded to uniform, however, the fibers became fused at higher concentration of 16 wt%. Increased β phase content and reduced α phase content were also observed after the addition of 8 wt% $Al(NO_3)_3 \cdot 9H_2O$. The maximized d_{33} value of -116 pm/V (pC/N) was obtained at 10 wt% $Al(NO_3)_3 \cdot 9H_2O$. Metal ions from the salt and water molecules both affected the dipole moment orientation of PVDF chain, via ion-dipole interaction and hydrogen bonding respectively, which improved the β phase formation. The hydrated salts used in these studies can be ionized in the solution, which makes it challenging to identify whether the dominant mechanism is ion-dipole or hydrogen bonding interaction.

Salts with dipole moments but limited ionization can also induce β phase nucleation. Yu et al. provided a thorough investigation on 3 types of salts, unionized salts with dipole moment close to 0 ($SnCl_4 \cdot 5H_2O$, $AlCl_3$, $Co(Ac)_2 \cdot 4H_2O$), weakly ionized salts ($CoCl_2 \cdot 6H_2O$, $CuCl_2 \cdot 2H_2O$, $MnCl_2 \cdot 4H_2O$) and strongly ionized salts ($LiCl \cdot H_2O$, $CaCl_2$, $Al(NO_3)_3 \cdot 9H_2O$) [111]. The unionized salts were found to have insignificant effect on β phase content or piezoelectric properties of the electrospun PVDF fibers. The addition of weakly ionized salts with dipole moment increased solution conductivity and facilitated dipole orientation of PVDF chains in electrospinning, achieving the highest piezoelectric response among the 3 types of salts examined. The improvement of piezoelectric properties with increased filler fraction met a limit at a relatively high concentration above which the solution conductivity was too strong to produce uniform fibers. The strongly ionized salts improved β phase content at low filler concentration. The highest voltage output from the weakly ionized salts almost tripled the highest voltage from the strongly ionized salts, while the optimal filler concentration of weakly ionized salts was around 10 times the optimal concentration of strongly ionized salts. In conclusion, salt fillers are effective in promoting β phase formation for the electrospun PVDF fibers, however, the piezoelectric response is limited at high concentrations.

6.3. Carbon-based and other conductive fillers

Graphene is a two-dimensional sheet of sp^2-hybridized carbon in a honeycomb lattice arrangement. Graphene oxide (GO) is oxidized form of graphene containing oxygen functional groups. Reduced graphene oxide (rGO) is GO with reduced oxygen content and much higher electrical conductivity. The potential of graphene, GO and rGO in improving piezoelectric properties of the electrospun PVDF fibers has been extensively explored. Wu and Chou discovered that addition of graphene yielded enhanced d_{33} value from 15.2 pC/N to 19.2 pC/N but reduced β phase content from 83% to 76% [116]. The higher d_{33} value was attributed to improved interfacial polarization arising from the conductive graphene fillers. Abolhasani et al. provided a more elaborate analysis on the graphene concentration, reporting that the β phase content increased from 77% to 83% after adding 0.1 wt% graphene but higher concentration caused the β phase content to decrease. [62]. At 0.1 wt%, the highest voltage obtained under an applied pressure of 0.2 MPa and frequency of 1 Hz was 7.9 V, as compared to 3.8 V produced from pure PVDF electrospun fibers. The higher boundary charge after adding a low concentration of conductive graphene filler was considered to promote formation of the β phase. The same optimal concentration (0.1 wt%) was reported in a different work when GO was added as the filler [117]. Abbasipour et al. conducted comparative studies on graphene and GO, while Ongun et al. compared GO and rGO [33,118,119]. The electrospun composite fibers produced with GO fillers showed larger diameters, higher dielectric constant, higher β phase content, and lower degree of crystallinity than fibers with graphene fillers. In comparison to the pure PVDF electrospun fibers which had d_{33} value of 17 pC/N and output voltage of 1 V under three-point bending with 5 mm displacement, the PVDF/graphene and PVDF/GO fibers with filler concentration of 1.6 wt% yielded d_{33} value of 18 pC/N and 24 pC/N, and output voltage of ~1.3 V and 2.1 V, respectively [33,118,119]**.** GO was concluded to be more effective than graphene in improving piezoelectric properties of the electrospun PVDF fibers. In terms of comparison between GO and rGO, the electrospun PVDF/rGO composite fibers were found to be more uniform with higher dielectric constant and higher β phase content than the PVDF/GO fibers. The PVDF/rGO fibers achieved maximum output voltage of 4.38 V with 0.8% (w/v) rGO while the PVDF/GO fibers achieved maximum output voltage of 1.15 V with 0.4% (w/v) GO, both measured by finger-tapping. While both materials showed substantial improvement in piezoelectricity than pure PVDF fibers (maximum voltage of

0.50 V), rGO was observed to be more effective than GO due to enhanced conductivity caused by lower amount of oxygen function groups on the surface.

Carbon nanotube (CNT) is tubular form of carbon atom sheet. Single-walled carbon nanotube (SWCNT) consists of a single carbon layer while multi-walled carbon nanotube (MWCNT) consists of multiple concentric carbon layers. MWCNT has been used as a filler for electrospun PVDF fibers. Ahn et al. characterized the crystalline structure of electrospun PVDF composite fibers containing functionalized MWCNT at low concentration of 0.05-1 wt% [17]. They discovered that the β phase content increased from 35% to 41.9% after adding 0.05 wt% MWCNT, and the increment plateaued to 44.8-44.9% at MWCNT concentration of 0.5-1.0 wt%. The interaction between the carboxylic acid groups on the functionalized MWCNT and the CF_2 dipoles of PVDF chains was considered as the mechanism to enhance β phase formation. Yu et al. looked into higher concentration of MWCNT (3-10 wt%) [86]. The pure PVDF electrospun fibers possessed degree of crystallinity of 31% and β phase content of 54.8%. Under buckling loading (longitudinal displacement 3 cm, frequency 0.8 Hz) in a configuration where the two ends of the sample were clamped, the output voltage was ~2 V. In comparison, the best piezoelectric property of the electrospun composite fibers was observed at 5 wt% MWCNT, with degree of crystallinity of 38.1%, β phase content of 68.4%, and output voltage of 6 V under the same buckling load. The improvement of piezoelectric properties with addition of MWCNT was also confirmed by Wu et al. by fabricating aligned electrospun PVDF composite fibers [40]. The β phase content increased slightly from 88% to 89%, d_{33} value from 27.4 pC/N to 31.3 pC/N, output sensitivity from 1.93 mV/N to 2.26 mV/N under compressive load, and output sensitivity from 3.45 mV/percentage strain to 4.29 mV/percentage strain under tensile deformation.

SWCNT has higher aspect ratio and smaller diameter than MWCNT. However, unlike MWCNT, fewer studies have been conducted on SWCNT as a filler for electrospun PVDF fibers. Yee et al. investigated how different surface chemistry of SWCNT may affect β phase formation [120]. Delocalized π electrons of SWCNT could interact with the fluorine atoms of PVDF to facilitate β conformation. At low concentration of 0.01 wt%, SWCNT with hydroxyl groups had a more pronounced effect on nucleating β crystallites due to hydrogen bond formation. On the other hand, SWCNT with ester groups interacted with PVDF chains via weaker dipole-dipole interaction. Huang et al. further showed that compared with MWCNT, SWCNT yielded similar improvement on β formation, but slightly higher electrical conductivity, better filler alignment and higher degree of crystal orientation [121] . These results indicate SWCNT is a promising candidate for improving the piezoelectric properties of PVDF, which demands further research.

Although incomparable to graphene or CNT in terms of electrical conductivity, polyaniline (PANi) is a conductive filler that can improve the charge transportation in electrospun PVDF fibers. Cai et al. demonstrated that adding PANi had a significant effect on converting α phase to β phase [122]. The β phase content increased with PANi concentration in the range of 0-9.69 wt%. Khalifa et al. reported that PANi was not a nucleating agent but a filler to improve the electrical conductivity [58]. After adding 17.5 wt% PANi, the β phase content increased from 34.9% to 40.9% but degree of crystallinity decreased from 38.9% to 37.4%. The authors explained that the improvement in β phase content was due to enhanced stretching facilitated by higher electrical conductivity of the jet.

6.4. Noble metal fillers

Noble metals, such as platinum or silver, do not possess piezoelectric properties but their anticorrosive and antioxidative properties in humid condition can enhance mechanical stability of the generator made from electrospun PVDF fibers [34]. The incorporation of noble metal as fillers can also induce crystallization of β phase through the interaction between the charged surface of the metal fillers and the dipoles of PVDF. Platinum (Pt) is one example of noble metal fillers. Ghosh and Mandal fabricated electrospun PVDF composite fibers with 1.5 wt% Pt-salt [34]. They defined a quantity called the degree of crystallinity of β phase as the product of β phase content and total degree of crystallinity. Including Pt in the aligned electrospun PVDF fibers caused increase in the degree of crystallinity of β phase from 37% to 55%, d_{33} value from ~22 pC/N to ~44 pC/N and maximum output voltage from 0.2 V to 0.4 V under a compressive force (7 N, frequency 5 Hz).

Silver nanowire (AgNW) or silver nanoparticle (AgNP) have been analyzed for its influence on β phase nucleation of electrospun PVDF fibers. Li et al. fabricated PVDF composite fibers with the addition of AgNW up to 3 wt% [123]. The best piezoelectric properties were obtained at 1.5 wt% AgNW, with increased d_{33} value (29.8 pC/N) compared with the pure PVDF fiber (d_{33} of 18.1 pC/N). The authors ascribed the improvement to interaction between the electron-rich surface of AgNW and the $-CH_2$ dipoles of PVDF. Issa et al. further investigated AgNP at low concentration of 0-1 wt% [124]. The pure PVDF fibers exhibited β phase content of ~76% and output voltage of 0.15 V under vibration with frequency of 35 Hz. At 0.4-0.6 wt% filler concentration, the PVDF/AgNP composite fibers showed enhancement in dielectric constant and β phase content (~81%). The highest output voltage of 2 V was obtained for 0.4 wt% AgNP, under vibration at frequency of 30 Hz. Based on their work, Wu and Chou provided a more detailed analysis on the effect of soundwave with different frequencies on the piezoelectric response of the electrospun PVDF/AgNP composite fibers, targeting the application of acoustic-electric conversion [125]. They reported β phase content of 94% and d_{33} value of 27.1 pC/N at the optimal AgNP concentration of 1 wt%. For such composite fibers subjected to vibration, the maximum output voltage was 59.2 mV at low frequency (100-400 Hz), 55.8 mV at medium frequency (315-1250 Hz), and 34.0 mV at high frequency (1250-5000 Hz). On account of the antibacterial properties of silver, electrospun PVDF/AgNP composite fibers can be further explored in smart textile or biomedical energy-harvesting applications [126].

Recently emerged noble metals open up more research capacity of piezoelectric materials. Examples include MXene and Borophene, which are advanced 2D materials synthesized in 2010s [127]. There still be limited works applying these noble metals on piezoelectric polymers. Zhao et al. fabricated MXene-loaded PVDF film with improvement in d_{33} value from 21 pC/N for pure PVDF to 43 pC/N at 0.4 wt% of MXene [128]. The voltage sensitivity of MXene/PVDF sensor reached 0.0480 V/N with applied force of 50-300 N carried out with force hammer test. The enhancement of piezoelectric properties was subscribed to substantial increase in conductivity due to MXene loading. Future works on using these noble metals as fillers for improving piezoelectric properties of electrospun PVDF fibers may facilitate manufacturing of new generation of smart textiles.

6.5. Natural Biodegradable fillers

Fillers from natural biodegradable polymers with good piezoelectric properties have been examined to understand if they can promote β or γ phase formation of electrospun PVDF fibers. Natural fillers are generally non-toxic, renewable, and favored in textile applications. Cellulose nanocrystal (CNC) or cellulose fiber is an example of such fillers. CNCs are rod-like structures with high aspect ratio, superior mechanical properties, and abundant hydroxyl groups. The hydroxyl groups tend to form hydrogen bonds with the electronegative fluorine atoms in PVDF so that CNC can induce nucleation of electroactive crystalline phases for PVDF [129]. Issa et al. used cellulose fibers up to 4 wt% to produce electrospun PVDF composite fibers with diameter of 370-870 nm [130]. The degree of crystallinity decreased from 34.3% to 33.4% after 0.5 wt% cellulose fibers was added, then increased with cellulose fiber concentration, up to 35.8% at 4 wt%. However, the β phase content did not change after adding cellulose fibers. Similar trend was observed by Fashandi et al., who demonstrated that low CNC loading (1 wt%) resulted in larger fiber diameter (718 nm, compared to 439 nm for pure PVDF fibers) due to higher viscosity, lower degree of crystallinity (27.35%, compared to 31.24% for pure PVDF fibers) due to disappearance of α phase, and lower output voltage (2.1 V compared to 3.5 V for pure PVDF fibers) [131]. Higher concentration of CNC (5 wt%) reduced the fiber diameter (559 nm) on account of higher electrical conductivity, improved the degree of crystallinity (36.24%) and β phase formation, and produced better piezoelectric response (6.3 V). Different from these studies, Lizundia et al. reported that CNC at low concentration was effective, but at high concentration could restrict molecular chains from forming preferential crystalline structures due to aggregation [132]. Fu et al. also found that addition of 2 wt% CNC with average diameter of 15 nm (Figure 8a) improved the degree of crystallinity from 48.43% to 68.09% and β phase content from 85.08% to 89.96% compared with pure PVDF fibers, but increasing CNC concentration higher than 2 wt% showed negative effect on β phase formation and piezoelectric properties [133]. The morphology of the electrospun PVDF fibers at different loadings of CNC in Figure 8b-d showed uniform and bead-free fibers. The generator fabricated from the PVDF composite fibers with 2 wt% CNC produced the highest output voltage of ~60 V upon cyclic bending (Figure 8e).

Chitin, a linear polysaccharide with intrinsic molecular polarization due to its α and β polymorphs, is another type of piezoelectric natural polymer [134]. Chitin on its own can be electrospun into aligned fibers with average diameter of ~150 nm and output voltage of 0.1 V per 1 kPa applied force [135]. Incorporating chitin nanofibers in PVDF solution to cast films can substantially improve the piezoelectric properties due to hydrogen bonding between chitin and PVDF, yielding β phase content of 81%, d_{33} value of 35.56 pC/N, and output voltage of 49 V [136]. Adding chitin nanowhiskers with average length of ~225 nm and width of ~15 nm as filler to electrospin PVDF composite fibers has been demonstrated to show improvement in oil-water separation and dye removal, but not in piezoelectric applications [137,138]. Future work can be conducted on analyzing if chitin nanowhisker is an effective filler for enhancing the piezoelectric properties of the electrospun PVDF fibers.

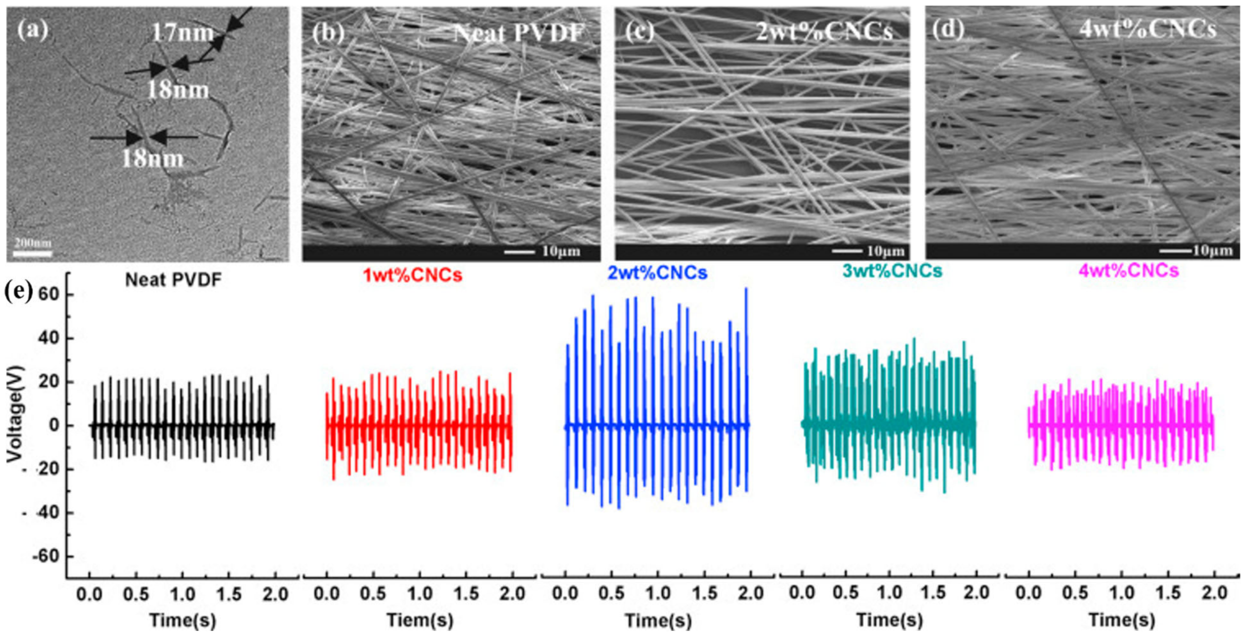

Figure 8. Morphology of (a) CNC rods, (b) electrospun PVDF fibers, (c) PVDF fibers with 2 wt% CNC, (d) PVDF fibers with 4 wt% CNC, (e) output voltages of generators produced from electrospun PVDF with different CNC loadings. Reproduced from Material Letters, Fu et al., 187, Improved piezoelectric properties of electrospun poly(vinylidene fluoride) fibers blended with cellulose nanocrystals, 86-88, 2017, with permission from Elsevier.

6.6. Hydrophilic fillers

Some hydrophilic fillers possess large amount of hydroxyl groups on the surface, which can orient the dipoles of PVDF to form ordered electroactive crystalline structures. Hydrophilic nanosilica is one such example. Haddadi et al. provided a systematic analysis on the effect of hydrophilic nanosilica (up to 2 wt%) on electrospun PVDF fibers [139]. The average fiber diameter increased with the concentration of hydrophilic nanosilica. At the optimal concentration of 0.5 wt%, the electrospun composite fibers showed the highest β phase content of 83.99% (51.62% at 0 wt%), degree of crystallinity of 28.3% (32.7% at 0 wt%), and output voltage of 1.771 V at an applied force of 13.9 N (corresponding data for 0 wt% was 1.122 V at 12.75 N). To further identify the significance of hydrophilicity in improving piezoelectric properties of PVDF, Haddadi et al. compared the hydrophilic and hydrophobic nanosilica [19]. The hydrophobic nanosilica exhibited more agglomeration on the surface of electrospun PVDF fibers. Under the same applied force, both electrospun PVDF composite fibers containing hydrophobic and hydrophilic nanosilica produced higher output voltage than pure PVDF fibers, with more pronounced improvement provided by the hydrophilic nanosilica. While these works have demonstrated hydrophilic property of nanosilica is effective in improving piezoelectric properties of electrospun PVDF fibers, the enhancement by hydrophobic nanosilica should be further investigated to understand the full capacity of this filler.

6.7. Clay

Mixing nanoclay in PVDF has been investigated in thermal treatment (e.g. annealing, melt-quenching, etc.) of solution casted composite films since charge (ion)-dipole attraction of exfoliated nanoclay layers with negative charges and positive dipoles of PVDF promote heterogeneous nucleation of β and γ phases [140]. Regardless of the temperature, the type and concentration of nanoclay both affect the crystalline structure of PVDF. Lopes et al. compared 3 types of nanoclay, montmorillonite, laponite and kaolinite, and obtained PVDF composite with decreasing electroactive phase content in that order [141]. The authors ascribed the trend to the nature of nanoclay, where the molecular interlayers in montmorillonite and laponite could expand more significantly than kaolinite. They further reported that increasing nanoclay concentration from 0.10 wt% to 0.25 wt% changed d_{33} value from 0 to -7 pC/N. Their observations indicated effectiveness of nanoclay in improving piezoelectric properties of PVDF.

Addition of nanoclay in PVDF to fabricate electrospun composite fibers has also been attempted. Yoon and Kelarakis blended 1 wt% Lucentite organically modified nanoclay with PVDF solution to yield electrospun composite fibers that had increased β phase and disappeared α phase compared to pure PVDF fibers [142]. Lucentite nanoclay also promoted more uniform fiber morphology due to increased viscosity and electrical conductivity of the mixture. The same phenomenon of converting beaded morphology to uniform fibers was observed by Xin et al. by including 5 wt% Nanomer® I.44P nanoclay in PVDF fibers [143]. With increased β phase content, a maximum voltage of 2.76 V was achieved for the PVDF/nanoclay composite fibers in a cantilever damping test, compared to 1.65 V achieved for the pure PVDF fibers. To further explain how concentration of nanoclay affected the fiber morphology and piezoelectric properties, Khalifa et al. provided a comprehensive analysis on the inclusion of halloysite nanotube (HNT), a kaolinite nanoclay with tubular structure [144]. Raising the HNT concentration from 0 wt% to 20 wt% promoted production of uniform fibers with smaller diameter. The β phase content increased linearly from 34.6% to 81.1% as the HNT loading was increased from 0 wt% to 10 wt%, but higher loading reduced the β phase content. Enhancement in β phase content was attributed to negative charge-CH_2 dipole interaction between HNT and PVDF. However, addition of HNT showed a negative influence on the degree of crystallinity, which was believed to be caused by rod-like HNT restricting the mobility of polymer chains. The maximum output voltage of 955 mV was obtained at 10 wt% HNT under a compressive load of 100 g, compared to ~300 mV obtained for pure PVDF fibers. The output voltage of generators produced from the electrospun PVDF/nanoclay composite fibers was at a relatively low level (<5 V) until Tiwari et al. reported superior piezoelectric performance of electrospun PVDF/Cloisite® 30B nanoclay fibers [145]. They investigated the effect of 0-20 wt% Cloisite® 30B nanoclay, an organically modified montmorillonite nanoclay, and reported morphology change from beads to uniform fibers after 15 wt% Cloisite® 30B nanoclay was added. The highest output voltages obtained for this composite fiber was 70 V via finger tapping and 5.1 V under impulse, and its β phase content was 79%. Higher filler concentration of 20 wt% led to formation of beads, decreased β phase content, and lower voltage output. The magnitude of the load or strain used to measure the piezoelectric responses was not reported in this work. In conclusion, nanoclay acts as a nucleating agent to promote β phase formation and is effective in improving the piezoelectric responses of the electrospun PVDF composite fibers for a range of filler concentration (~10-15 wt%).

7. Effect of Defects

7.1. Morphological and structural defects

Morphological defects that may exist electrospun PVDF fibers caused by unoptimized electrospinning parameters can pose negative effect on their piezoelectric performance. The dominant morphological defect is the failure to form uniform cylindrical fibers. Examples include bead structures, nonuniform fiber diameters, grooved fibers, cracks, porous cross-sections, as well as porous and/or rough surfaces [53,67]. Coarse fiber surfaces and porous structures can result from phase separation induced by nonuniform evaporation of solvent from exterior or interior [67]. Beads are generally formed when the parameters for electrospinning or preparing the polymer solution are not optimized, leading to unbalanced surface tension, jet charges, and electrostatic forces required to produce smooth cylindrical fibers. Large variations in fiber diameter and porous internal structure affect uniformity in the formation of PVDF chains formation and weaken the piezoelectric properties [53]. For smart textile applications, reduced β phase formation caused by morphological defects is detrimental to the piezoelectric performance of electrospun PVDF fibers. However, morphological defects such as porous structures are considered beneficial in absorption-related applications due to the increased specific area of fibers and hence more absorption sites [67].

Structural defects of electrospun PVDF fibers include undesired chain conformation or low crystallinity. Although β phase is the preferred chain arrangement, α phase is energetically more stable [146]. Since α phase is non-polar, a high α phase composition can be avoided by optimizing electrospinning and solution parameters, addition of fillers, or post-treatments that supply additional poling, stretching, or heating for β phase formation [85,147]. It should be pointed out that an increase in the total degree of crystallinity may not directly correlate with enhanced piezoelectric performance, as the formation of more α phase can also lead to higher crystallinity. Thus, even at a high degree of total crystallinity, structural defects such as the lack of β phase can still result in poor piezoelectric properties [133].

7.2. Device defects

When electrospun PVDF fibers are fabricated into energy or sensing devices, the piezoelectric output can be influenced by a number of other factors [9,10]. Electrospun fibers are well known for their high surface area to volume ratio, which provides strong contact with the electrode layers. However, when the electrodes are exposed to an environment with high humidity, the device can experience short circuiting and become incapable of transferring energy harvested by the device [9]. Humidity and rapid temperature change can also affect the charge transfer across the interfaces between fibers and electrodes. To alleviate the impacts on piezoelectric performance from the surroundings, an insulation layer is generally applied to ensure steady energy output [10]. This additional component, however, adversely affects the wearability of the device in smart textile applications and raises the manufacturing cost. An alternative approach was proposed by Gao et al., involving an overall core-shell design where the electrospun PVDF fibers wrap around flexible electrodes [80]. For a device with multilayer structures, delamination can arise from weak interfacial contact between different fiber layers [80]. Finally, a direct circuit printing on PVDF is difficult because the melting temperature of PVDF is only around 171-175°C and the electrospun fiber mat does not possess a completely flat surface [10]. On account of these challenges, energy devices produced from electrospun PVDF fibers have a relatively low power output, which remains an obstacle for their commercial applications.

8. ML Analysis

For electrospun polymeric fibers, ML has been employed to analyze the effect of electrospinning parameters on fiber diameter, mechanical properties, electrochemical properties, etc. [148] However, to the authors' knowledge, such analyses have not been conducted to predict the voltage response of electrospun PVDF fibers under applied deformation or force, with or without fillers.

8.1. ML setup

To conduct ML analysis on the piezoelectric response of electrospun PVDF composite fibers, 315 data were collected from various papers which reported the open-circuit output voltages. The output voltages were grouped into 4 classes in Table 2 based on the typical operational voltage of electronics, disregarding the current output. While acknowledging that current rating is required to power these electronic applications, current output is not taken into account when evaluating voltage classifications due to the lack of current measurement in considerable number of works.

Table 2. Classification of output voltage ranges based on electronic applications [149,150]

Class	Value (V)	Potential Applications
1	<1.8	Not suitable for electronics
2	1.8-5	Can be used for LED
3	5-12	Can be used for small-scale electronics, such as headset, MP3, etc.
4	>12	Can be used for large-scale electronics, such as laptop, portable DVD player, etc.

The collected data contained output voltage produced from two types of excitation sources, deformation and applied force. Thus, the data were divided into two categories, force-induced voltage and strain-induced voltage. The force-induced voltage refers to the output voltage generated by compression or impact force, thus one input variable is the applied force. The strain-induced voltage refers to the voltage generated by bending or tensile deformation, with strain calculated using methods listed in Section 3 as one input variable. The effects of 39 experimental variables, including electrospinning parameters, solution properties, filler properties and fiber properties, on the output voltage were assessed. To reduce the variable dimension, the correlations between the experimental variables and the voltage classes were evaluated using Spearman's ρ, a non-parametric statistical method [151]. The results of feature selection are shown in Figure 9. The significant parameters with 99% confidence interval (p-value<0.01), besides the excitation sources, were identified. For the force-induced voltage, the significant parameters were MWCNT, $BaTiO_3$, HNT, filler concentration, and electric field. MWCNT, $BaTiO_3$ and HNT represented the fillers with high electrical conductivity, high piezoelectric coefficient, and ability to promote β phase content of PVDF, respectively. For the strain-induced voltage, the significant parameters were PVDF concentration, MWCNT, $BaTiO_3$, HNT, filler concentration, flow rate, and electric field. These parameters, combined with either strain or force, were selected as the inputs for training the ML models to predict the output voltage range of the electrospun PVDF composite fibers.

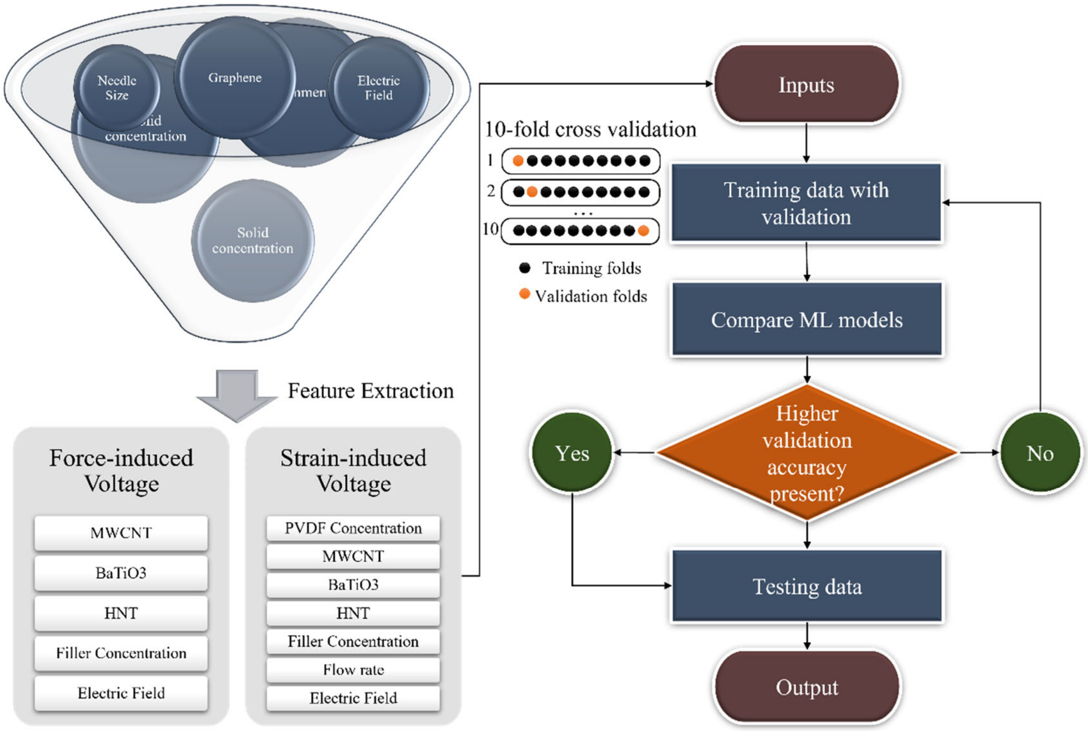

Figure 9. Process to select ML model for voltage output from input variables.

Classification Learner in MATLAB R2021b was used with training and testing procedures illustrated in Figure 10. The strain-induced voltage and force-induced voltage data were both separated into training dataset with validation (80%) and test dataset (20%). 10-fold cross validation was conducted on the training data for validation before testing. Specifically, the training data were partitioned into 10 random subsets with 9 subsets used for training and 1 subset used for validation. The process was repeated 10 times by alternating the validation subset. The validation process was used to evaluate the accuracy of the model as the hyperparameters, the ML parameters which controlled the training process, were tuned. The test process assessed the accuracy of the model after the model was finalized to indicate if the predictions were valid. The classification models used are listed in Figure 10 with their advantages and disadvantages.

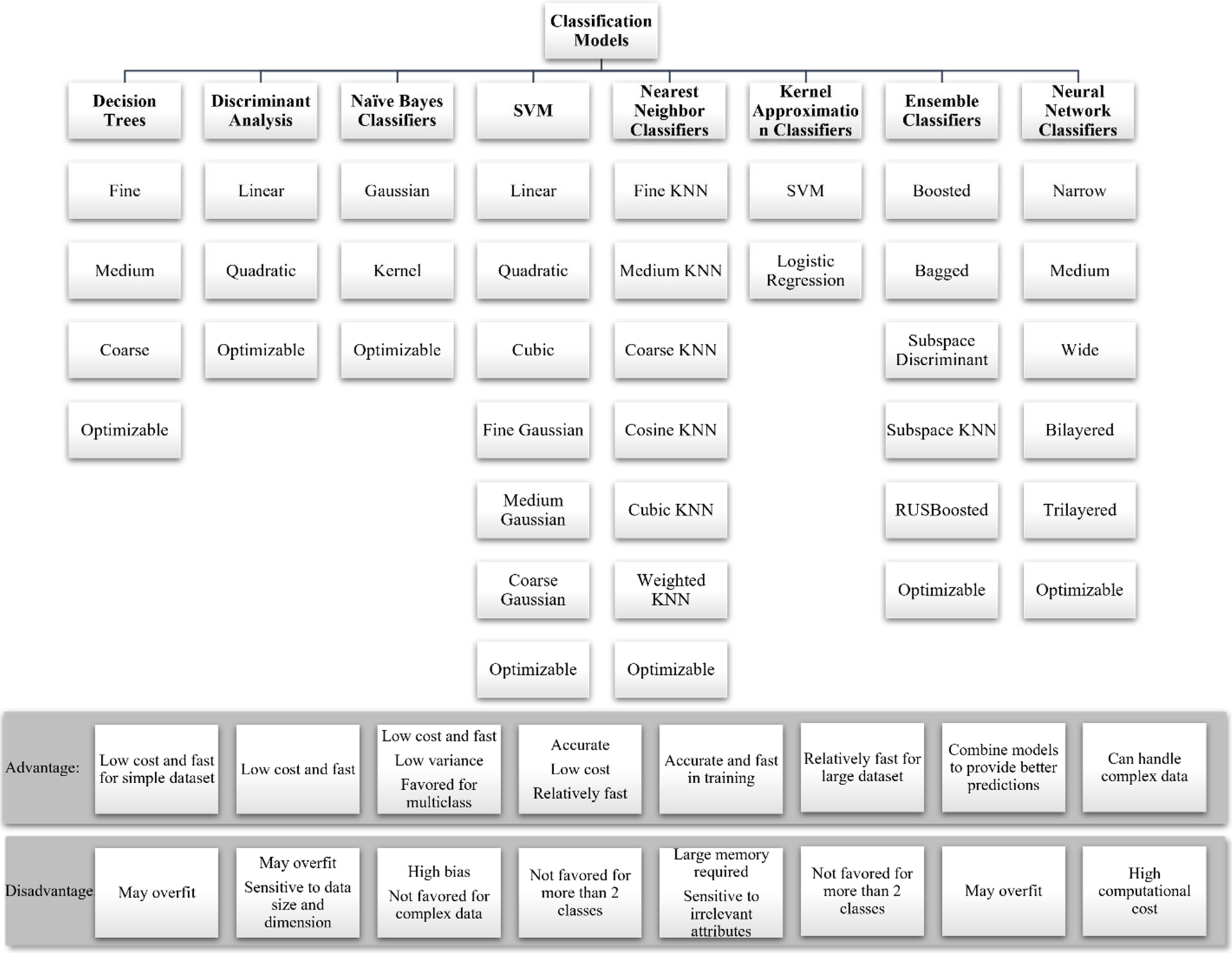

Figure 10. ML models adopted in Classification Learner of MATLAB with advantages and disadvantages.

8.2. ML Results

The classification models were compared based on validation accuracy, prediction speed, training time, and test accuracy. The models with the highest validation accuracy or highest test accuracy to predict the force-induced and strain-induced voltages are summarized in Table 3. The hyperparameters used in these models were optimized with MATLAB Classification Learner and are listed in Table 4. For force-induced voltage, Boosted Trees, which was AdaBoost algorithm combined with Decision Tree leaners, showed the highest validation accuracy of 80.6%. The test accuracy exhibited a slight decrement to 76.2%. Weighted KNN classifier had a lower validation accuracy of 75.3% but a substantially higher test accuracy of 90.5%. It also showed an almost 3-

fold increase in prediction speed and 6-fold reduction in training time, when compared with Boosted Trees. For strain-induced voltage, the highest validation accuracy of 88.7% was obtained from Logistic Regression Kernel classifier, with its test accuracy further increasing to 91.7%. The highest test accuracy of 95.8% was achieved with Fine Gaussian SVM classifier with a slightly reduced prediction speed but more than 2-fold decrease in training time.

Table 3. Classification models with the highest validation accuracy or test accuracy for force-induced voltage and strain-induced voltage.

	Force-induced		Strain-induced	
Method	Boosted Trees	Weighted KNN	Logistic Regression Kernel	Fine Gaussian SVM
Validation accuracy	80.6	75.3	88.7	84.5
Prediction speed (observations/sec)	1200	3400	2400	2100
Training time (sec)	6.2	1.0	2.0	0.8
Test accuracy (%)	76.2	90.5	91.7	95.8

Table 4. Hyperparameters used for the Classification models.

	Force-induced		Strain-induced	
Method	Boosted Trees	Weighted KNN	Logistic Regression Kernel	Fine Gaussian SVM
Hyperparameters	Ensemble method: AdaBoost Maximum number of splits: 20 Number of learners: 30 Learning rate: 0.1	Number of neighbors: 10 Distance metric: Euclidean Distance weight: Squared inverse Standardize data: true	Multiclass method: One-vs-One Iteration limit: 1000	Kernel function: Gaussian Kernel scale: 0.71 Box constraint level: 1 Multiclass method: One-vs-One Standardize data: true

Figure 11 shows, for force-induced voltage, the scatter plots of how the output voltage class changes with the significant parameters, as predicted by the models. For each filler, “0” indicates that the filler is not added to the electrospun PVDF fibers while “1” indicates the filler is added. Darker color corresponds to overlapping data and hence more frequent occurrence. In both Boosted Trees and Weighted KNN classifiers, higher voltage class occurred at higher input force and after the addition of MWCNT. The majority of class 1 voltage occurred at low electric field and before the addition of $BaTiO_3$. These trends agreed with the summarized results in Sections 5 and 6. At high electric field, finer fibers were generated which promoted PVDF to crystallize into electroactive phases. Addition of $BaTiO_3$ enhanced the overall piezoelectric properties of the electrospun composite fibers. Inclusion of MWCNT improved the electron charge transfer leading to increase in the piezoelectric response. For filler concentration, the majority of class 4 and class 1 voltages were located at low weight ratio, but most data were randomly scattered. This suggests the need to optimize the filler concentration, and the loading limit is likely different for different fillers depending on how they interact with PVDF. HNT was not as effective as $BaTiO_3$ or MWCNT in terms of improving the piezoelectric properties of the electrospun PVDF fibers.

For the strain-induced voltages predicted by Logistic Regression Kernel and Fine Gaussian SVM classifiers, the scatter plots are presented in Figure 12 for the significant parameters. High voltage class was achieved at low electric field, high applied strain, low flow rate, and after addition of $BaTiO_3$ and MWCNT. For the dataset adopted to conduct ML analysis on strain-induced voltage, high electric field might have caused jet instability and posed negative effect on forming electroactive crystallites. In terms of flow rate, while maintaining uniform jet formation, reducing flow rate could increase the charge density over the jet surface, yield thinner fibers, and increase β phase content. High voltage class was observed at intermediate PVDF concentrations and filler weight ratios, suggesting that optimal concentrations of PVDF and fillers exist and overloading can pose negative influence on the piezoelectric response of the fabricated fibers. Similar to force-induced voltages, addition of $BaTiO_3$ or MWCNT was beneficial in improving the piezoelectric properties, while no clear relationship was detected between the voltage class and the addition of HNT. In both Figure 11 and Figure 12, the voltage class increased with the applied force or strain. Therefore, voltage sensitivity, which is the ratio between output voltage and the applied force or strain, should be reported to more accurately evaluate the piezoelectric response of the electrospun PVDF and PVDF composite fibers.

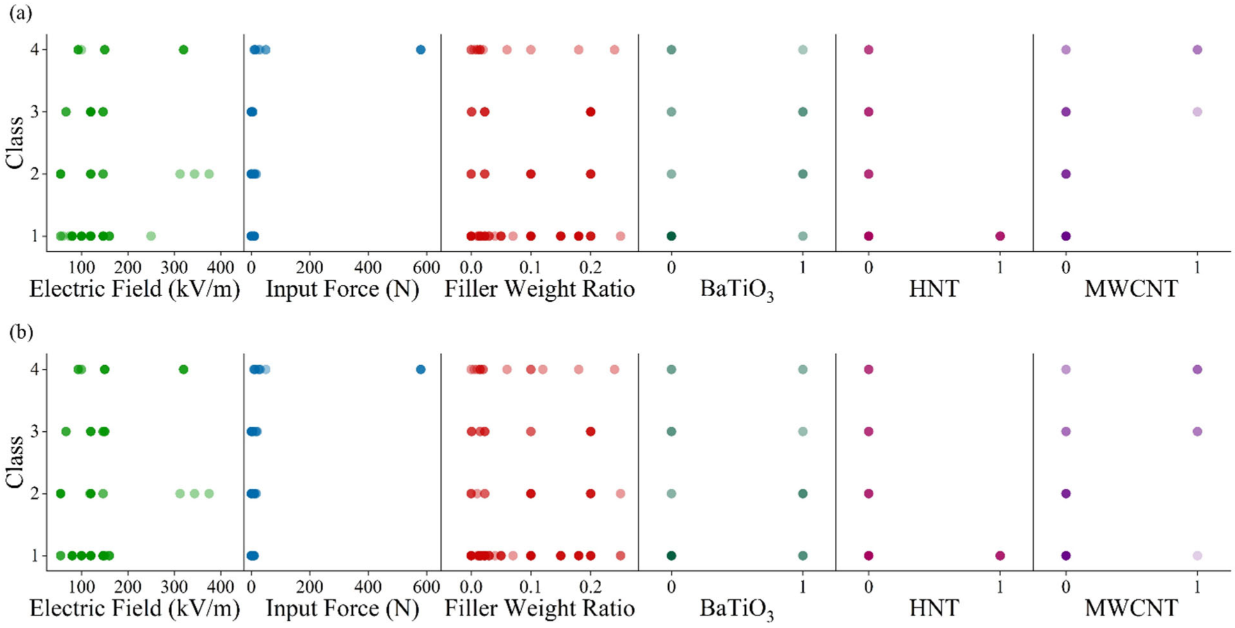

Figure 11. Scatter plots of force-induced voltage class vs electric field, input force, filler weight ratio (filler concentration), BaTiO3, HNT, and MWCNT, respectively; predicted by (a) Boosted Trees classifier and (b) Weighted KNN classifier.

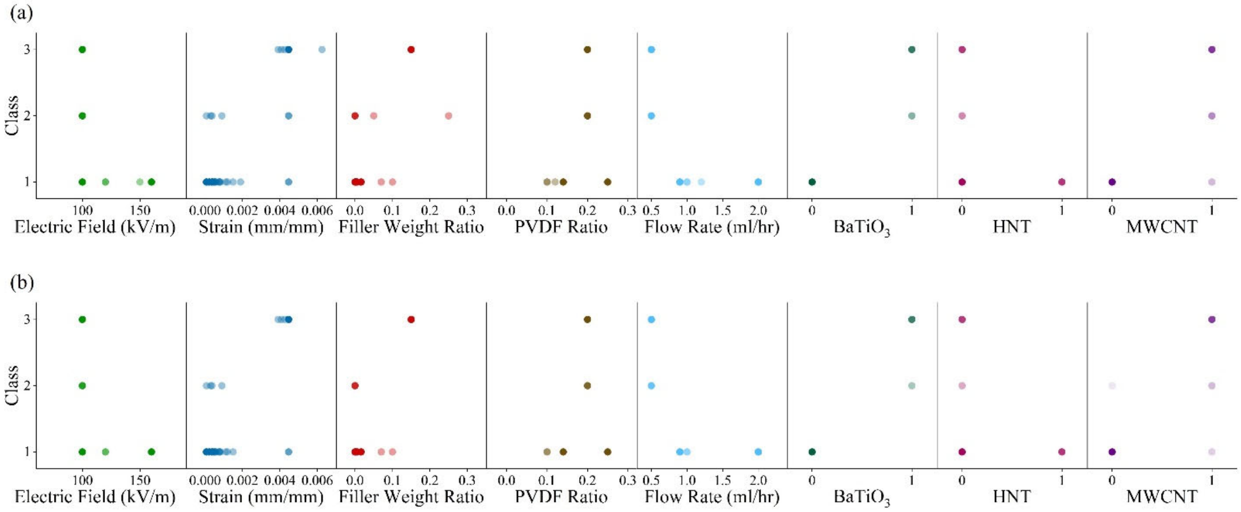

Figure 12. Scatter plots of strain-induced voltage class vs electric field, strain, filler weight ratio, PVDF concentration in solution, flow rate, BaTiO3, HNT, and MWCNT, respectively; predicted by (a) Logistic Regression Kernel classifier and (b) Fine Gaussian SVM classifier.

The performance evaluation of the chosen models is shown in Figure 13 using confusion matrices. True positive rate (TPR) and false negative rate (FNR) are respectively the fractions of correctly and incorrectly assigned observations per true class. For instance, in the validation results of Boosted Trees classifier for estimating force-induced voltage (Figure 13a), 92.8% of the output voltages were correctly assigned to class 1 while 3.1%, 3.1%, and 1.0% of the voltages were incorrectly assigned to classes 2, 3, and 4. That resulted in TPR of 92.8% and FNR of 7.2%. After testing (Figure 13b), TPR of class 1 slightly reduced to 92%, causing the test accuracy to be slightly smaller than the validation accuracy. In the validation results of Weighted KNN classifier (Figure 13c), the lowest TPR of 50% occurred for class 2, indicating prediction of force-induced output voltages in class 2 was not as accurate as the prediction of voltages in other classes. In the testing results (Figure 13d), TPR for class 2 reduced but TPR for classes 1, 3, and 4 reached 100%, which confirmed high agreement between the model prediction and the actual output voltage class.

The strain-induced voltage was assigned into 3 classes because the reported output voltages did not reach the range of class 4 as specified in Table 2. In the validation results of Logistic Regression Kernel classifier (Figure 13e), the highest TPR of 98.5% was achieved for class 1 and the highest FNR of 60% occurred for class 2. For the test results (Figure 13f), TPR of class 1 and 3 increased up to 100% and the highest FNR (class 2) reduced to 50%. Fine Gaussian SVM classifier showed lower TPR for classes 1 and 3 in additional to higher FNR for class 2 than Logistic Regression Kernel classifier, in the validation results (Figure 13g). However, the test accuracy of Fine Gaussian SVM classifier (Figure 13h) was the highest among the four classifiers, with 100% TPR achieved for classes 1 and 3, and 25% FNR for class 2. In general, the classification models for strain-induced voltage estimation were able to achieve 100% accuracy in assigning voltages to classes 1 and 3 with slightly lower accuracy for class 2 output voltage.

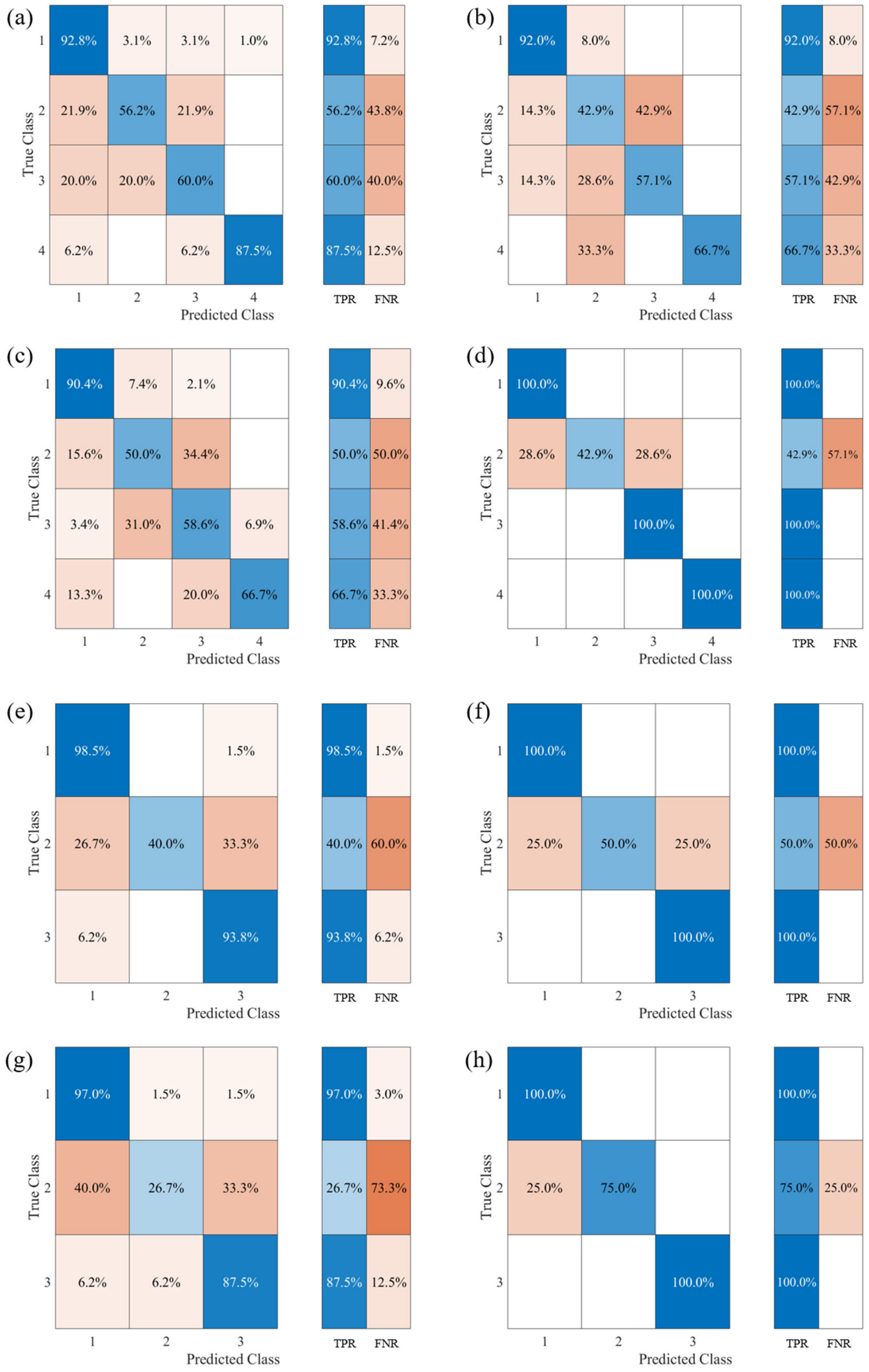

(a)

True Class	1	2	3	4	TPR	FNR
1	92.8%	3.1%	3.1%	1.0%	92.8%	7.2%
2	21.9%	56.2%	21.9%		56.2%	43.8%
3	20.0%	20.0%	60.0%		60.0%	40.0%
4	6.2%		6.2%	87.5%	87.5%	12.5%

Predicted Class

(b)

True Class	1	2	3	4	TPR	FNR
1	92.0%	8.0%			92.0%	8.0%
2	14.3%	42.9%	42.9%		42.9%	57.1%
3	14.3%	28.6%	57.1%		57.1%	42.9%
4		33.3%		66.7%	66.7%	33.3%

Predicted Class

(c)

True Class	1	2	3	4	TPR	FNR
1	90.4%	7.4%	2.1%		90.4%	9.6%
2	15.6%	50.0%	34.4%		50.0%	50.0%
3	3.4%	31.0%	58.6%	6.9%	58.6%	41.4%
4	13.3%		20.0%	66.7%	66.7%	33.3%

Predicted Class

(d)

True Class	1	2	3	4	TPR	FNR
1	100.0%				100.0%	
2	28.6%	42.9%	28.6%		42.9%	57.1%
3			100.0%		100.0%	
4				100.0%	100.0%	

Predicted Class

(e)

True Class	1	2	3	TPR	FNR
1	98.5%		1.5%	98.5%	1.5%
2	26.7%	40.0%	33.3%	40.0%	60.0%
3	6.2%		93.8%	93.8%	6.2%

Predicted Class

(f)

True Class	1	2	3	TPR	FNR
1	100.0%			100.0%	
2	25.0%	50.0%	25.0%	50.0%	50.0%
3			100.0%	100.0%	

Predicted Class

(g)

True Class	1	2	3	TPR	FNR
1	97.0%	1.5%	1.5%	97.0%	3.0%
2	40.0%	26.7%	33.3%	26.7%	73.3%
3	6.2%	6.2%	87.5%	87.5%	12.5%

Predicted Class

(h)

True Class	1	2	3	TPR	FNR
1	100.0%			100.0%	
2	25.0%	75.0%		75.0%	25.0%
3			100.0%	100.0%	

Predicted Class

Figure 13. Confusion matrices for (a) validation results and (b) test results of Boosted Trees classifier; (c) validation results and (d) test results of Weighted KNN classifier; (e) validation results and (f) test results of Logistic Regression Kernel classifier; (g) validation results and (h) test results of Fine Gaussian SVM classifier.

8.3. Comparative analysis and future perspectives

From recent publications, electrospun PVDF fibers with high piezoelectric output are summarized in Tables 5 and 6 for force-induced voltage and strain-induced voltage, respectively. As seen in Table 5, consistent with the predictions from ML, class 4 voltage mostly occurred at high electric field and high input force with majority of the filler weight ratio less than 0.2. ML identified BaTiO3 and MWCNT as beneficial additives that improve piezoelectric output, which were implemented in the two studies ranked #2 and #5.

The parameters that resulted in class 3 voltage (ranked #1) showed good agreement with ML prediction (Table 6): relatively low electric field, high strain, intermediate filler and PVDF concentrations, low flow rate, and after the addition of BaTiO3. It should be emphasized, however, that the voltage output is dependent on the applied stimuli (force or strain). By defining force-induced voltage sensitivity and strain-induced voltage sensitivity as the output voltage divided by applied force and applied strain, respectively (see Tables 5 and 6), it is evident that the voltage class is not directly correlated to voltage sensitivity. For instance, the study ranked #2 in Table 6 has a lower voltage class than the work ranked #1, but a higher strain-induced voltage sensitivity. This further highlights the necessity to standardize the piezoelectric output results and specify the applied force or strain when reporting the piezoelectric output.

Table 5. Ranking of force-induced voltage output reported in recent publications.

Rank	Voltage (V)	Force-induced voltage sensitivity (V/N)	Class	Electric field (kV/m)	Input force (N)	Filler weight ratio	Filler type	Ref
1	30.00	0.60	4	150	50	0.015	Platinum	[34]
2	21.31	0.04	4	320	580	0.18; 0.01	BaTiO3; MWCNT	[152]
3	24.60	1.77	4	93	13.9	0.005	Nanosilica	[139]
4	12.50	0.42	4	150	30	0.1	NaNbO3	[152]
5	12.00	7.53	4	120	1.594	0.2; 0.18	BaTiO3; ZnO	[153]

Table 6. Ranking of strain-induced voltage output reported in recent publications.

Rank	Voltage (V)	Strain-induced voltage sensitivity (V/(mm/mm))	Class	Electric field (kV/m)	Strain (mm/mm)	Filler weight ratio	PVDF concentration	Flow rate (ml/hr)	Filler type	Ref
1	11.00	2463.70	3	100	0.0045	0.150; 0.0015	0.2	0.5	BaTiO3; Graphene	[35]
2	2.30	6133.33	2	160	0.0004	0.016	0.14	2	GO	[33]
3	0.38	345.45	1	100	0.0011	0.005	0.25	0.9	Nickle Chloride Hexahydrate	[32]
4	0.08	152.00	1	28000	0.0005	0.000	0.18	N/A	N/A	[52]
5	0.03	0.26	1	N/A	0.1000	0.002	0.18	N/A	CNT	[40]

The application of electrospun PVDF fibers towards next-generation flexible self-powered generators and sensors is being extensively investigated. Recent studies have attempted address the drawbacks of low energy output of PVDF compared with piezoelectric ceramics by optimizing electrospinning procedure, solution parameters, and addition of fillers [68,99]. Other approaches include the modification of functional groups, consideration of regioisomerism, etc. Tackling such an intricate problem demands the processing of a large amount of data and the development of models that can accurately predict the piezoelectric performance of PVDF. ML is well-suited for this purpose. While the classification models used in the present work provide good prediction for the voltage class, a few other directions are suggested here. 1) Consider maximizing piezoelectric performance as an optimization target and integrate traditional optimization methods (e.g. Taguchi method, response surface methodology) with ML methods such as genetic algorithm, artificial neural network, support vector regression, etc. [154] 2) Establish the piezoelectric governing equations with independent variables and use deep energy methods derived from deep neural network to solve the equations [155]. 3) Implement reinforcement learning in adaptive manufacturing procedure to execute optimal control for maximal piezoelectric performance [156]. Exploiting the potential of ML to help achieve high piezoelectric performance of PVDF is becoming an effective and even a crucial path for the advancement of this class of smart materials.

Conclusion

Electrospun PVDF fibers with high aspect ratio have great potential in energy harvesting fields including e-textiles, piezoelectric biomedicine, nano-sensors and generators. A review is conducted on recent works that investigate the production of PVDF and PVDF-composite fibers by solution electrospinning. The effects of processing parameters and solution properties on crystallization structure formation and piezoelectric properties of the PVDF fibers are discussed. To produced PVDF-composite fibers, various fillers have been introduced, which can be categorized into piezoelectric ceramics, salts, conductive fillers, noble metal, natural fillers, hydrophilic fillers, and clay. These fillers enhance the piezoelectric properties of electrospun PVDF fibers through a range of mechanisms, such as high piezoelectric coefficient of the filler, enhancement of electron transfer by increasing conductivity, and promotion of β phase formation by dipole-dipole interaction, ion (charge)-dipole interactions, fluorine-π interactions, or radical reactions. Following the definition of 4 classes for output voltage produced by electrospun PVDF composite fibers, machine learning models are employed to estimate the voltage output from these composite fibers under force-induced or strain-induced deformation. Four models are identified that provide high accuracy in predicting output voltage class. These models can be used to select fillers or optimize electrospinning parameters in order to produce electrospun PVDF and PVDF composite fibers with high piezoelectric performance.

Conflict of Interest

The authors would like to declare that they no competing interest.

Acknowledgement

The authors acknowledged that this work is funded by Natural Sciences and Engineering Research Council of Canada (NSERC) [RGPIN-2018-04281 and RGPIN-2018-06309].

Data Availability

The raw/processed data required to reproduce these findings cannot be shared at this time as the data also forms part of an ongoing study.

References

[1] Wang S, Wang ZL, Yang YA. A one-structure-based hybridized nanogenerator for scavenging mechanical and thermal energies by triboelectric–piezoelectric–pyroelectric effects. Adv Mater 2016;28:2881–7.

[2] Shen D, Xiao M, Zou G, Liu L, Duley WW, Zhou YN. Self-powered wearable electronics based on moisture enabled electricity generation. Adv Mater 2018;30:1705925.

[3] Lu YJ, Shi ZF, Shan CX, Shen DZ. ZnO nanostructures and lasers. Nanoscale Semicond. Lasers, Elsevier; 2019, p. 75–108.

[4] Qing X, Li W, Wang Y, Sun H. Piezoelectric transducer-based structural health monitoring for aircraft applications. Sensors (Switzerland) 2019;19:1–27. https://doi.org/10.3390/s19030545.

[5] Huang Y, Chen J, Zhao M, Feng M. Electromechanical coupling characteristics of double-layer piezoelectric quasicrystal actuators. Int J Mech Sci 2021;196:106293. https://doi.org/10.1016/j.ijmecsci.2021.106293.

[6] Rödig T, Schönecker A, Gerlach G. A survey on piezoelectric ceramics for generator applications. J Am Ceram Soc 2010;93:901–12.

[7] Jordan TL, Ounaies Z. Piezoelectric ceramics characterization. INSTITUTE FOR COMPUTER APPLICATIONS IN SCIENCE AND ENGINEERING HAMPTON VA; 2001.

[8] Lam TN, Ma CY, Hsiao PH, Ko WC, Huang YJ, Lee SY, et al. Tunable mechanical and electrical properties of coaxial electrospun composite nanofibers of P(VDF-TRFE) and P(VDF-TRFE-CTFE). Int J Mol Sci 2021;22. https://doi.org/10.3390/ijms22094639.

[9] Lund A, Rundqvist K, Nilsson E, Yu L, Hagström B, Müller C. Energy harvesting textiles for a rainy day: woven piezoelectrics based on melt-spun PVDF microfibres with a conducting core. Npj Flex Electron 2018;2:1–9. https://doi.org/10.1038/s41528-018-0022-4.

[10] Azimi S, Golabchi A, Nekookar A, Rabbani S, Amiri MH, Asadi K, et al. Self-powered cardiac pacemaker by piezoelectric polymer nanogenerator implant. Nano Energy 2021;83:105781. https://doi.org/10.1016/j.nanoen.2021.105781.

[11] Bera B, Mandal D, Das Sarkar M. Sensor Made of PVDF/graphene Electrospinning Fiber and Comparison between Electrospinning PVDF Fiber and PVDF/graphene Fiber. Imp J

Interdiscip Res 2016;2:1411–3.

[12] Tamura T, Kawakami H. Membranes for Fuel Cell Electrolytes 2010:1324–8. https://doi.org/10.1021/nl1007079.

[13] Szewczyk PK, Gradys A, Kim SK, Persano L, Marzec M, Kryshtal A, et al. Enhanced Piezoelectricity of Electrospun Polyvinylidene Fluoride Fibers for Energy Harvesting. ACS Appl Mater Interfaces 2020;12:13575–83. https://doi.org/10.1021/acsami.0c02578.

[14] Hu X, Yi K, Liu J, Chu B. High Energy Density Dielectrics Based on PVDF-Based Polymers. Energy Technol 2018;6:849–64.

[15] Karan SK, Mandal D, Khatua BB. Self-powered flexible Fe-doped RGO/PVDF nanocomposite: An excellent material for a piezoelectric energy harvester. Nanoscale 2015;7:10655–66. https://doi.org/10.1039/c5nr02067k.

[16] Martín J, Zhao D, Lenz T, Katsouras I, De Leeuw DM, Stingelin N. Solid-state-processing of δ-PVDF. Mater Horizons 2017;4:408–14. https://doi.org/10.1039/c7mh00007c.

[17] Ahn Y, Lim JY, Hong SM, Lee J, Ha J, Choi HJ, et al. Enhanced piezoelectric properties of electrospun poly(vinylidene fluoride)/multiwalled carbon nanotube composites due to high β-phase formation in poly(vinylidene fluoride). J Phys Chem C 2013;117:11791–9. https://doi.org/10.1021/jp4011026.

[18] Barrau S, Ferri A, Da Costa A, Defebvin J, Leroy S, Desfeux R, et al. Nanoscale Investigations of α- And γ-Crystal Phases in PVDF-Based Nanocomposites. ACS Appl Mater Interfaces 2018;10:13092–9. https://doi.org/10.1021/acsami.8b02172.

[19] Haddadi SA, Ghaderi S, Amini M, Ramazani SAA. Mechanical and piezoelectric characterizations of electrospun PVDF-nanosilica fibrous scaffolds for biomedical applications. Mater Today Proc 2018;5:15710–6. https://doi.org/10.1016/j.matpr.2018.04.182.

[20] Pinto T V., Cardoso N, Costa P, Sousa CM, Durães N, Silva C, et al. Light driven PVDF fibers based on photochromic nanosilica@naphthopyran fabricated by wet spinning. Appl Surf Sci 2019;470:951–8. https://doi.org/10.1016/j.apsusc.2018.11.203.

[21] Lv R, Zhu Y, Liu H, Na B, Huang Y, Xie X. Poly(vinylidene fluoride)/poly(acrylonitrile) blend fibrous membranes by centrifugal spinning for high-performance lithium ion battery separators. J Appl Polym Sci 2017;134. https://doi.org/10.1002/app.44515.

[22] Liu W, Chen R, Ruan X, Fu X. Polymeric piezoelectric fiber with metal core produced by

electrowetting-aided dry spinning method. J Appl Polym Sci 2016;133.

[23] Doshi J, Reneker DH. Electrospinning process and applications of electrospun fibers. Conf Rec - IAS Annu Meet (IEEE Ind Appl Soc 1993;3:1698–703. https://doi.org/10.1109/ias.1993.299067.

[24] Yang W, Haoyi L. Principle and equipment of polymer melt differential electrospinning preparing ultrafine fiber. IOP Conf. Ser. Mater. Sci. Eng., vol. 64, IOP Publishing; 2014.

[25] Al-Dhahebi AM, Saheed MSM, Mustapha M. Effects of solution concentration on the synthesis of polyvinylidene fluoride (PVDF) electrospun nanofibers. Mater Today Proc 2021. https://doi.org/10.1016/j.matpr.2021.06.128.

[26] Dargahi J, Payandeh S, Parameswaran M. A micromachined piezoelectric teeth-like laparoscopic tactile sensor: theory, fabrication and experiments. Proc - IEEE Int Conf Robot Autom 1999;1:299–304. https://doi.org/10.1109/robot.1999.769995.

[27] Acciani G, Di Modugno F, Gelao G. Comparative Studies of Piezoelectric Harvester Devices. Energy Harvest Technol Methods Appl n.d.:1–18.

[28] Zhang Q, Liu S, Luo H, Guo Z, Hu X, Xiang Y. Hybrid capacitive/piezoelectric visualized meteorological sensor based on in-situ polarized PVDF-TrFE films on TFT arrays. Sensors Actuators, A Phys 2020;315:112286. https://doi.org/10.1016/j.sna.2020.112286.

[29] Wang YC, Chen YW. Application of piezoelectric PVDF film to the measurement of impulsive forces generated by cavitation bubble collapse near a solid boundary. Exp Therm Fluid Sci 2007;32:403–14. https://doi.org/10.1016/j.expthermflusci.2007.05.003.

[30] Wang R, Tang E, Yang G. Dynamic Piezoelectric Properties of PZT-5H Under Shock Compression. Phys Status Solidi 2019;216:1800859.

[31] Fang J, Wang X, Lin T. Electrical power generator from randomly oriented electrospun poly(vinylidene fluoride) nanofibre membranes. J Mater Chem 2011;21:11088–91. https://doi.org/10.1039/c1jm11445j.

[32] Dhakras D, Borkar V, Ogale S, Jog J. Enhanced piezoresponse of electrospun PVDF mats with a touch of nickel chloride hexahydrate salt. Nanoscale 2012;4:752–6. https://doi.org/10.1039/c2nr11841f.

[33] Abbasipour M, Khajavi R, Yousefi AA, Yazdanshenas ME, Razaghian F, Akbarzadeh A. Improving piezoelectric and pyroelectric properties of electrospun PVDF nanofibers using nanofillers for energy harvesting application. Polym Adv Technol 2019;30:279–91.

https://doi.org/10.1002/pat.4463.

[34] Ghosh SK, Mandal D. Synergistically enhanced piezoelectric output in highly aligned 1D polymer nanofibers integrated all-fiber nanogenerator for wearable nano-tactile sensor. Nano Energy 2018;53:245–57. https://doi.org/10.1016/j.nanoen.2018.08.036.

[35] Shi K, Sun B, Huang X, Jiang P. Synergistic effect of graphene nanosheet and BaTiO3 nanoparticles on performance enhancement of electrospun PVDF nanofiber mat for flexible piezoelectric nanogenerators. Nano Energy 2018;52:153–62. https://doi.org/10.1016/j.nanoen.2018.07.053.

[36] ZOHOOR H, KHORSANDIJOU SM, ABEDINNASAB MH. Modified Nonlinear 3D Euler Bernoulli Beam Theory. J Syst Des Dyn 2008;2:1170–82. https://doi.org/10.1299/jsdd.2.1170.

[37] Li Y, Lee DK, Kim JY, Kim B, Park NG, Kim K, et al. Highly durable and flexible dye-sensitized solar cells fabricated on plastic substrates: PVDF-nanofiber-reinforced TiO2 photoelectrodes. Energy Environ Sci 2012;5:8950–7. https://doi.org/10.1039/c2ee21674d.

[38] Tiwari MK, Yarin AL, Megaridis CM. Electrospun fibrous nanocomposites as permeable, flexible strain sensors. J Appl Phys 2008;103. https://doi.org/10.1063/1.2885112.

[39] Persano L, Dagdeviren C, Su Y, Zhang Y, Girardo S, Pisignano D, et al. High performance piezoelectric devices based on aligned arrays of nanofibers of poly(vinylidenefluoride-co-trifluoroethylene). Nat Commun 2013;4:1610–33. https://doi.org/10.1038/ncomms2639.

[40] Wu CM, Chou MH, Zeng WY. Piezoelectric response of aligned electrospun polyvinylidene fluoride/carbon nanotube nanofibrous membranes. Nanomaterials 2018;8:1–13. https://doi.org/10.3390/nano8060420.

[41] Deng W, Yang T, Jin L, Yan C, Huang H, Chu X, et al. Cowpea-structured PVDF/ZnO nanofibers based flexible self-powered piezoelectric bending motion sensor towards remote control of gestures. Nano Energy 2019;55:516–25. https://doi.org/10.1016/j.nanoen.2018.10.049.

[42] Alam MM, Ghosh SK, Sultana A, Mandal D. An Effective Wind Energy Harvester of Paper Ash-Mediated Rapidly Synthesized ZnO Nanoparticle-Interfaced Electrospun PVDF Fiber. ACS Sustain Chem Eng 2018;6:292–9. https://doi.org/10.1021/acssuschemeng.7b02441.

[43] Garain S, Jana S, Sinha TK, Mandal D. Design of in Situ Poled Ce3+-Doped Electrospun

PVDF/Graphene Composite Nanofibers for Fabrication of Nanopressure Sensor and Ultrasensitive Acoustic Nanogenerator. ACS Appl Mater Interfaces 2016;8:4532–40. https://doi.org/10.1021/acsami.5b11356.

[44] Mutsuda H, Kawakami K, Kurokawa T, Doi Y, Tanaka Y. A technology of electrical energy generated from ocean power using flexible piezoelectric device. Proc Int Conf Offshore Mech Arct Eng - OMAE 2010;3:313–21. https://doi.org/10.1115/OMAE2010-20103.

[45] Lee TH, Chen CY, Tsai CY, Fuh YK. Near-field electrospun piezoelectric fibers as sound-sensing elements. Polymers (Basel) 2018;10:1–10. https://doi.org/10.3390/polym10070692.

[46] Jiang J, Tu S, Fu R, Li J, Hu F, Yan B, et al. Flexible Piezoelectric Pressure Tactile Sensor Based on Electrospun BaTiO3/Poly(vinylidene fluoride) Nanocomposite Membrane. ACS Appl Mater Interfaces 2020;12:33989–98. https://doi.org/10.1021/acsami.0c08560.

[47] Chen F, Wu Y, Ding Z, Xia X, Li S, Zheng H, et al. A novel triboelectric nanogenerator based on electrospun polyvinylidene fluoride nanofibers for effective acoustic energy harvesting and self-powered multifunctional sensing. Nano Energy 2019;56:241–51. https://doi.org/10.1016/j.nanoen.2018.11.041.

[48] Lim J, Kim HS. Effects of SWCNT/PVDF composite web behavior on acoustic piezoelectric property. Sensors Actuators, A Phys 2021;330:112840. https://doi.org/10.1016/j.sna.2021.112840.

[49] Toda M, Thompson ML. Contact-type vibration Sensors using curved clamped PVDF film. IEEE Sens J 2006;6:1170–7. https://doi.org/10.1109/JSEN.2006.881407.

[50] Lee B, Park B, Yang H, Han JW, Choong C, Bae J, et al. Effects of substrate on piezoelectricity of electrospun poly (vinylidene fluoride)-nanofiber-based energy generators. ACS Appl Mater Interfaces 2014;6:3520–7.

[51] Bae JH, Chang SH. A new approach to fabricate poly(vinylidene fluoride-trifluoroethylene) fibers using a torsion-stretching method and characterization of their piezoelectric properties. Compos Part B Eng 2016;99:112–20. https://doi.org/10.1016/j.compositesb.2016.06.037.

[52] Liu ZH, Pan CT, Lin LW, Huang JC, Ou ZY. Direct-write PVDF nonwoven fiber fabric energy harvesters via the hollow cylindrical near-field electrospinning process. Smart

Mater Struct 2014;23. https://doi.org/10.1088/0964-1726/23/2/025003.

[53] Liu ZH, Pan CT, Lin LW, Lai HW. Piezoelectric properties of PVDF/MWCNT nanofiber using near-field electrospinning. Sensors Actuators, A Phys 2013;193:13–24. https://doi.org/10.1016/j.sna.2013.01.007.

[54] Chang C, Tran VH, Wang J, Fuh YK, Lin L. Direct-write piezoelectric polymeric nanogenerator with high energy conversion efficiency. Nano Lett 2010;10:726–31. https://doi.org/10.1021/nl9040719.

[55] Chen C, Bai Z, Cao Y, Dong M, Jiang K, Zhou Y, et al. Enhanced piezoelectric performance of BiCl3/PVDF nanofibers-based nanogenerators. Compos Sci Technol 2020;192:108100. https://doi.org/10.1016/j.compscitech.2020.108100.

[56] Ryu C, Hajra S, Sahu M, Jung SI, Jang IR, Kim HJ. PVDF-bismuth titanate based self-powered flexible tactile sensor for biomechanical applications. Mater Lett 2021;309:131308. https://doi.org/10.1016/j.matlet.2021.131308.

[57] Mokhtari F, Shamshirsaz M, Latifi M, Asadi S. Comparative evaluation of piezoelectric response of electrospun PVDF (polyvinilydine fluoride) nanofiber with various additives for energy scavenging application. J Text Inst 2017;108:906–14. https://doi.org/10.1080/00405000.2016.1202091.

[58] Khalifa M, Mahendran A, Anandhan S. Durable, efficient, and flexible piezoelectric nanogenerator from electrospun PANi/HNT/PVDF blend nanocomposite. Polym Compos 2019;40:1663–75. https://doi.org/10.1002/pc.24916.

[59] Martins P, Lopes AC, Lanceros-Mendez S. Electroactive phases of poly(vinylidene fluoride): Determination, processing and applications. Prog Polym Sci 2014;39:683–706. https://doi.org/10.1016/j.progpolymsci.2013.07.006.

[60] Cai X, Lei T, Sun D, Lin L. A critical analysis of the α, β and γ phases in poly(vinylidene fluoride) using FTIR. RSC Adv 2017;7:15382–9. https://doi.org/10.1039/c7ra01267e.

[61] Barstugan R, Barstugan M, Ozaytekin I. PBO/graphene added β-PVDF piezoelectric composite nanofiber production. Compos Part B Eng 2019;158:141–8. https://doi.org/10.1016/j.compositesb.2018.09.059.

[62] Abolhasani MM, Shirvanimoghaddam K, Naebe M. PVDF/graphene composite nanofibers with enhanced piezoelectric performance for development of robust nanogenerators. Compos Sci Technol 2017;138:49–56.

[63] Hussein AD, Sabry RS, Abdul Azeez Dakhil O, Bagherzadeh R. Effect of Adding BaTiO3 to PVDF as Nano Generator. J Phys Conf Ser 2019;1294:0–10. https://doi.org/10.1088/1742-6596/1294/2/022012.

[64] Jin L, Zheng Y, Liu ZK, Li JS, Yi YPQ, Fan YY, et al. Enhancement of β-Phase Crystal Content of Poly(vinylidene fluoride) Nanofiber Web by Graphene and Electrospinning Parameters. Chinese J Polym Sci (English Ed 2020;38:1239–47. https://doi.org/10.1007/s10118-020-2428-4.

[65] Singh RK, Lye SW, Miao J. Holistic investigation of the electrospinning parameters for high percentage of β-phase in PVDF nanofibers. Polymer (Guildf) 2021;214. https://doi.org/10.1016/j.polymer.2020.123366.

[66] Ribeiro C, Sencadas V, Ribelles JLG, Lanceros-Méndez S. Influence of processing conditions on polymorphism and nanofiber morphology of electroactive poly(vinylidene fluoride) electrospun membranes. Soft Mater 2010;8:274–87. https://doi.org/10.1080/1539445X.2010.495630.

[67] Zaarour B, Zhu L, Huang C, Jin X. Controlling the Secondary Surface Morphology of Electrospun PVDF Nanofibers by Regulating the Solvent and Relative Humidity. Nanoscale Res Lett 2018;13. https://doi.org/10.1186/s11671-018-2705-0.

[68] Gade H, Nikam S, Chase GG, Reneker DH. Effect of electrospinning conditions on β-phase and surface charge potential of PVDF fibers. Polymer (Guildf) 2021;228. https://doi.org/10.1016/j.polymer.2021.123902.

[69] Shao H, Fang J, Wang H, Lang C, Lin T. Robust Mechanical-to-Electrical Energy Conversion from Short-Distance Electrospun Poly(vinylidene fluoride) Fiber Webs. ACS Appl Mater Interfaces 2015;7:22551–7. https://doi.org/10.1021/acsami.5b06863.

[70] Gee S, Johnson B, Smith AL. Optimizing electrospinning parameters for piezoelectric PVDF nanofiber membranes. J Memb Sci 2018;563:804–12.

[71] Jiyong H, Yuanyuan G, Hele Z, Yinda Z, Xudong Y. Effect of electrospinning parameters on piezoelectric properties of electrospun PVDF nanofibrous mats under cyclic compression. J Text Inst 2018;109:843–50. https://doi.org/10.1080/00405000.2017.1377882.

[72] Jiyong H, Yinda Z, Hele Z, Yuanyuan G, Xudong Y. Mixed effect of main electrospinning parameters on the β-phase crystallinity of electrospun PVDF nanofibers. Smart Mater

Struct 2017;26. https://doi.org/10.1088/1361-665X/aa7245.

[73] Tian D, He CH, He JH. Macromolecule orientation in nanofibers. Nanomaterials 2018;8. https://doi.org/10.3390/nano8110918.

[74] Shuakat MN, Lin T. Direct electrospinning of nanofibre yarns using a rotating ring collector. J Text Inst 2016;107:791–9. https://doi.org/10.1080/00405000.2015.1061785.

[75] Edmondson D, Cooper A, Jana S, Wood D, Zhang M. Centrifugal electrospinning of highly aligned polymer nanofibers over a large area. J Mater Chem 2012;22:18646–52. https://doi.org/10.1039/c2jm33877g.

[76] Lei T, Xu Z, Cai X, Xu L, Sun D. New Insight into Gap Electrospinning: Toward Meter-long Aligned Nanofibers. Langmuir 2018;34:13788–93. https://doi.org/10.1021/acs.langmuir.8b03114.

[77] Sharafkhani S, Kokabi M. Ultrathin-shell PVDF/CNT nanocomposite aligned hollow fibers as a sensor/actuator single element. Compos Sci Technol 2020;200:108425. https://doi.org/10.1016/j.compscitech.2020.108425.

[78] Baji A, Mai Y, Du X, Wong S. Improved Tensile Strength and Ferroelectric Phase Content of Self-Assembled Polyvinylidene Fluoride Fiber Yarns. Macromol Mater Eng 2012;297:209–13.

[79] Peng H, Wu M, Wang Y, Li T, Sun F, Lou C, et al. Enhancing piezoelectricity of poly (vinylidene fluoride) nano-wrapped yarns with an innovative yarn electrospinning technique. Polym Int 2021;70:851–9.

[80] Gao H, Minh PT, Wang H, Minko S, Locklin J, Nguyen T, et al. High-performance flexible yarn for wearable piezoelectric nanogenerators. Smart Mater Struct 2018;27:95018.

[81] Zaarour B, Zhu L, Huang C, Jin X. Fabrication of a polyvinylidene fluoride cactus-like nanofiber through one-step electrospinning. RSC Adv 2018;8:42353–60. https://doi.org/10.1039/c8ra09257e.

[82] Huang F, Wei Q, Wang J, Cai Y, Huang Y. Effect of temperature on structure, morphology and crystallinity of PVDF nanofibers via electrospinning. E-Polymers 2008:1–8. https://doi.org/10.1515/epoly.2008.8.1.1758.

[83] Zaarour B, Zhu L, Jin X. Controlling the surface structure, mechanical properties, crystallinity, and piezoelectric properties of electrospun PVDF nanofibers by maneuvering

molecular weight. Soft Mater 2019;17:181–9. https://doi.org/10.1080/1539445X.2019.1582542.

[84] Ma J, Larsen RM. Use of Hansen solubility parameters to predict dispersion and strain transfer of functionalized single-walled carbon nanotubes in poly(vinylidene fluoride) composites. J Thermoplast Compos Mater 2014;27:801–15. https://doi.org/10.1177/0892705712455036.

[85] Cozza ES, Monticelli O, Marsano E, Cebe P. On the electrospinning of PVDF: Influence of the experimental conditions on the nanofiber properties. Polym Int 2013;62:41–8. https://doi.org/10.1002/pi.4314.

[86] Yu H, Huang T, Lu M, Mao M, Zhang Q, Wang H. Enhanced power output of an electrospun PVDF/MWCNTs-based nanogenerator by tuning its conductivity. Nanotechnology 2013;24. https://doi.org/10.1088/0957-4484/24/40/405401.

[87] Costa LMM, Bretas RES, Gregorio R. Effect of Solution Concentration on the Electrospray/Electrospinning Transition and on the Crystalline Phase of PVDF. Mater Sci Appl 2010;01:247–52. https://doi.org/10.4236/msa.2010.14036.

[88] Saha S, Yauvana V, Chakraborty S, Sanyal D. Synthesis and characterization of polyvinylidene-fluoride (PVDF) nanofiber for application as piezoelectric force sensor. Mater Today Proc 2019;18:1450–8.

[89] Bottino A, Capannelli G, Munari S, Turturro A. Solubility parameters of poly (vinylidene fluoride). J Polym Sci Part B Polym Phys 1988;26:785–94.

[90] Smallwood I. Handbook of organic solvent properties. Butterworth-Heinemann; 2012.

[91] Karaki T, Adachi M, Yan K. High-performance lead-free barium titanate piezoelectric ceramics. Adv. Sci. Technol., vol. 54, Trans Tech Publ; 2008, p. 7–12.

[92] Hao J, Li W, Zhai J, Chen H. Progress in high-strain perovskite piezoelectric ceramics. Mater Sci Eng R Reports 2019;135:1–57. https://doi.org/10.1016/j.mser.2018.08.001.

[93] Gao J, Xue D, Liu W, Zhou C, Ren X. Recent progress on BaTiO3-based piezoelectric ceramics for actuator applications. Actuators, vol. 6, Multidisciplinary Digital Publishing Institute; 2017, p. 24.

[94] Algueró M, Ricote J, Hungría T, Castro A. High-sensitivity piezoelectric, low-tolerance-factor perovskites by mechanosynthesis. Chem Mater 2007;19:4982–90. https://doi.org/10.1021/cm071656v.

[95] Maeder MD, Damjanovic D, Setter N. Lead free piezoelectric materials. J Electroceramics 2004;13:385–92. https://doi.org/10.1007/s10832-004-5130-y.

[96] Chamankar N, Khajavi R, Yousefi AA, Rashidi A, Golestanifard F. A flexible piezoelectric pressure sensor based on PVDF nanocomposite fibers doped with PZT particles for energy harvesting applications. Ceram Int 2020;46:19669–81. https://doi.org/10.1016/j.ceramint.2020.03.210.

[97] Koç M, Paralı L, Şan O. Fabrication and vibrational energy harvesting characterization of flexible piezoelectric nanogenerator (PEN) based on PVDF/PZT. Polym Test 2020;90. https://doi.org/10.1016/j.polymertesting.2020.106695.

[98] Du X, Zhou Z, Zhang Z, Yao L, Zhang Q, Yang H. Porous, multi-layered piezoelectric composites based on highly oriented PZT/PVDF electrospinning fibers for high-performance piezoelectric nanogenerators. J Adv Ceram 2022;11:331–44. https://doi.org/10.1007/s40145-021-0537-3.

[99] Guo W, Tan C, Shi K, Li J, Wang XX, Sun B, et al. Wireless piezoelectric devices based on electrospun PVDF/BaTiO3 NW nanocomposite fibers for human motion monitoring. Nanoscale 2018;10:17751–60. https://doi.org/10.1039/c8nr05292a.

[100] Teka A, Bairagi S, Shahadat M, Joshi M, Ziauddin Ahammad S, Wazed Ali S. Poly(vinylidene fluoride) (PVDF)/potassium sodium niobate (KNN)–based nanofibrous web: A unique nanogenerator for renewable energy harvesting and investigating the role of KNN nanostructures. Polym Adv Technol 2018;29:2537–44. https://doi.org/10.1002/pat.4365.

[101] Bairagi S, Ali SW. Influence of High Aspect Ratio Lead-Free Piezoelectric Fillers in Designing Flexible Fibrous Nanogenerators: Demonstration of Significant High Output Voltage. Energy Technol 2019;7:1900538.

[102] Setasuwon P, Vaneesorn N, Kijamnajsuk S, Thanaboonsombut A. Nanocrystallization of Bi0.5Na0.5TiO3 piezoelectric material. Sci Technol Adv Mater 2005;6:278–81. https://doi.org/10.1016/j.stam.2005.03.005.

[103] Liu J, Yu D, Zheng Z, Huangfu G, Guo Y. Lead-free BiFeO3 film on glass fiber fabric: Wearable hybrid piezoelectric-triboelectric nanogenerator. Ceram Int 2021;47:3573–9. https://doi.org/10.1016/j.ceramint.2020.09.205.

[104] Qin W, Zhou P, Xu X, Irshad MS, Qi Y, Zhang T. Enhanced output performance of

piezoelectric energy harvester based on hierarchical Bi3.15Nd0.85Ti3O12 microspheres/PVDF-HFP composite. Sensors Actuators A Phys 2022;333:113307. https://doi.org/10.1016/j.sna.2021.113307.

[105] Gao PX, Lao CS, Ding Y, Wang ZL. Metal/semiconductor core/shell nanodisks and nanotubes. Adv Funct Mater 2006;16:53–62. https://doi.org/10.1002/adfm.200500301.

[106] Bafqi MSS, Bagherzadeh R, Latifi M. Fabrication of composite PVDF-ZnO nanofiber mats by electrospinning for energy scavenging application with enhanced efficiency. J Polym Res 2015;22:1–9. https://doi.org/10.1007/s10965-015-0765-8.

[107] Ma J, Zhang Q, Lin K, Zhou L, Ni Z. Piezoelectric and optoelectronic properties of electrospinning hybrid PVDF and ZnO nanofibers. Mater Res Express 2018;5. https://doi.org/10.1088/2053-1591/aab747.

[108] Satthiyaraju M, Ramesh T. Nanomechanical, Mechanical Responses and Characterization of Piezoelectric Nanoparticle-Modified Electrospun PVDF Nanofibrous Films. Arab J Sci Eng 2019;44:5697–709. https://doi.org/10.1007/s13369-018-03694-6.

[109] Li J, Chen S, Liu W, Fu R, Tu S, Zhao Y, et al. High Performance Piezoelectric Nanogenerators Based on Electrospun ZnO Nanorods/Poly(vinylidene fluoride) Composite Membranes. J Phys Chem C 2019;123:11378–87. https://doi.org/10.1021/acs.jpcc.8b12410.

[110] Fu Y, Cheng Y, Chen C, Li D, Zhang W. Study on preparation process and enhanced piezoelectric performance of pine-needle-like ZnO@PVDF composite nanofibers. Polym Test 2022;108:107513. https://doi.org/10.1016/j.polymertesting.2022.107513.

[111] Yu B, Mao M, Yu H, Huang T, Zuo W, Wang H, et al. Enhanced Piezoelectric Performance of Electrospun Polyvinylidene Fluoride Doped with Inorganic Salts. Macromol Mater Eng 2017;302:1–8. https://doi.org/10.1002/mame.201700214.

[112] Zhang D, Zhang X, Li X, Wang H, Sang X, Zhu G, et al. Enhanced piezoelectric performance of PVDF/BiCl3/ZnO nanofiber-based piezoelectric nanogenerator. Eur Polym J 2021:110956.

[113] Mokhtari F, Shamshirsaz M, Latifi M. Investigation of β phase formation in piezoelectric response of electrospun polyvinylidene fluoride nanofibers: LiCl additive and increasing fibers tension. Polym Eng Sci 2016;56:61–70.

[114] Mokhtari F, Shamshirsaz M, Latifi M, Foroughi J. Nanofibers-based piezoelectric energy

harvester for self-powered wearable technologies. Polymers (Basel) 2020;12:2697.

[115] Yousry YM, Yao K, Chen S, Liew WH, Ramakrishna S. Mechanisms for Enhancing Polarization Orientation and Piezoelectric Parameters of PVDF Nanofibers. Adv Electron Mater 2018;4. https://doi.org/10.1002/aelm.201700562.

[116] Wu CM, Chou MH. Sound absorption of electrospun polyvinylidene fluoride/graphene membranes. Eur Polym J 2016;82:35–45. https://doi.org/10.1016/j.eurpolymj.2016.07.001.

[117] Issa AA, Al-Maadeed MAAS, Mrlík M, Luyt AS. Electrospun PVDF graphene oxide composite fibre mats with tunable physical properties. J Polym Res 2016;23. https://doi.org/10.1007/s10965-016-1126-y.

[118] Zeyrek Ongun M, Oguzlar S, Doluel EC, Kartal U, Yurddaskal M. Enhancement of piezoelectric energy-harvesting capacity of electrospun β-PVDF nanogenerators by adding GO and rGO. J Mater Sci Mater Electron 2020;31:1960–8. https://doi.org/10.1007/s10854-019-02715-w.

[119] Abbasipour M, Khajavi R, Yousefi AA, Yazdanshenas ME, Razaghian F. The piezoelectric response of electrospun PVDF nanofibers with graphene oxide, graphene, and halloysite nanofillers: a comparative study. J Mater Sci Mater Electron 2017;28:15942–52. https://doi.org/10.1007/s10854-017-7491-4.

[120] Yee WA, Kong J, Zhang C, Liu T, Kotaki M, Lu X. Polymorphism of electrospun polyvinylidene difluoride/carbon nanotube (CNT) nanocomposites: Synergistic effects of CNT surface chemistry, extensional force and supercritical carbon dioxide treatment. Polymer (Guildf) 2012;53:5097–102. https://doi.org/10.1016/j.polymer.2012.08.044.

[121] Huang S, Yee WA, Tjiu WC, Liu Y, Kotaki M, Boey YCF, et al. Electrospinning of polyvinylidene difluoride with carbon nanotubes: Synergistic effects of extensional force and interfacial interaction on crystalline structures. Langmuir 2008;24:13621–6. https://doi.org/10.1021/la8024183.

[122] Cai X, Huang X, Zheng Z, Xu J, Tang X, Lei T. Effect of Polyaniline (Emeraldine Base) Addition on α to β Phase Transformation in Electrospun PVDF Fibers. J Macromol Sci Part B Phys 2017;56:75–82. https://doi.org/10.1080/00222348.2016.1270730.

[123] Li B, Zheng J, Xu C. Silver nanowire dopant enhancing piezoelectricity of electrospun PVDF nanofiber web. Fourth Int Conf Smart Mater Nanotechnol Eng 2013;8793:879314. https://doi.org/10.1117/12.2026758.

[124] Issa A, Al-Maadeed M, Luyt A, Ponnamma D, Hassan M. Physico-Mechanical, Dielectric, and Piezoelectric Properties of PVDF Electrospun Mats Containing Silver Nanoparticles. C 2017;3:30. https://doi.org/10.3390/c3040030.

[125] Wu CM, Chou MH. Acoustic–electric conversion and piezoelectric properties of electrospun polyvinylidene fluoride/silver nanofibrous membranes. Express Polym Lett 2020;14:103–14. https://doi.org/10.3144/expresspolymlett.2020.10.

[126] Marques SM, Carvalho I, Henriques M, Polcar T, Carvalho S. PVD-grown antibacterial Ag-TiN films on piezoelectric PVDF substrates for sensor applications. Surf Coatings Technol 2015;281:117–24. https://doi.org/10.1016/j.surfcoat.2015.09.057.

[127] Chaudhary V, Kaushik A, Furukawa H, Khosla A. Review—Towards 5th Generation AI and IoT Driven Sustainable Intelligent Sensors Based on 2D MXenes and Borophene. ECS Sensors Plus 2022;1:013601. https://doi.org/10.1149/2754-2726/ac5ac6.

[128] Zhao Q, Yang L, Ma Y, Huang H, He H, Ji H, et al. Highly sensitive, reliable and flexible pressure sensor based on piezoelectric PVDF hybrid film using MXene nanosheet reinforcement. J Alloys Compd 2021;886:161069. https://doi.org/10.1016/j.jallcom.2021.161069.

[129] Venkatesan M, Chen WC, Cho CJ, Veeramuthu L, Chen LG, Li KY, et al. Enhanced piezoelectric and photocatalytic performance of flexible energy harvester based on CsZn0.75Pb0.25I3/CNC–PVDF composite nanofibers. Chem Eng J 2021:133620. https://doi.org/10.1016/j.cej.2021.133620.

[130] Issa AA, Al-Maadeed M, Luyt AS, Mrlik M, Hassan MK. Investigation of the physico-mechanical properties of electrospun PVDF/cellulose (nano)fibers. J Appl Polym Sci 2016;133. https://doi.org/10.1002/app.43594.

[131] Fashandi H, Abolhasani MM, Sandoghdar P, Zohdi N, Li Q, Naebe M. Morphological changes towards enhancing piezoelectric properties of PVDF electrical generators using cellulose nanocrystals. Cellulose 2016;23:3625–37. https://doi.org/10.1007/s10570-016-1070-3.

[132] Lizundia E, Reizabal A, Costa CM, Maceiras A, Lanceros-Méndez S. Electroactive γ-Phase, Enhanced Thermal and Mechanical Properties and High Ionic Conductivity Response of Poly (Vinylidene Fluoride)/Cellulose Nanocrystal Hybrid Nanocomposites. Materials (Basel) 2020;13:743.

[133] Fu R, Chen S, Lin Y, Zhang S, Jiang J, Li Q, et al. Improved piezoelectric properties of electrospun poly(vinylidene fluoride) fibers blended with cellulose nanocrystals. Mater Lett 2017;187:86–8. https://doi.org/10.1016/j.matlet.2016.10.068.

[134] Kim K, Ha M, Choi B, Joo SH, Kang HS, Park JH, et al. Biodegradable, electro-active chitin nanofiber films for flexible piezoelectric transducers. Nano Energy 2018;48:275–83. https://doi.org/10.1016/j.nanoen.2018.03.056.

[135] Street RM, Huseynova T, Xu X, Chandrasekaran P, Han L, Shih WY, et al. Variable piezoelectricity of electrospun chitin. Carbohydr Polym 2018;195:218–24. https://doi.org/10.1016/j.carbpol.2018.04.086.

[136] Hoque NA, Thakur P, Biswas P, Saikh MM, Roy S, Bagchi B, et al. Biowaste crab shell-extracted chitin nanofiber-based superior piezoelectric nanogenerator. J Mater Chem A 2018;6:13848–58. https://doi.org/10.1039/c8ta04074e.

[137] Gopi S, Balakrishnan P, Pius A, Thomas S. Chitin nanowhisker (ChNW)-functionalized electrospun PVDF membrane for enhanced removal of Indigo carmine. Carbohydr Polym 2017;165:115–22. https://doi.org/10.1016/j.carbpol.2017.02.046.

[138] Gopi S, Kargl R, Kleinschek KS, Pius A, Thomas S. Chitin nanowhisker – Inspired electrospun PVDF membrane for enhanced oil-water separation. J Environ Manage 2018;228:249–59. https://doi.org/10.1016/j.jenvman.2018.09.039.

[139] Haddadi SA, Ahmad Ramazani SA, Talebi S, Fattahpour S, Hasany M. Investigation of the Effect of Nanosilica on Rheological, Thermal, Mechanical, Structural, and Piezoelectric Properties of Poly(vinylidene fluoride) Nanofibers Fabricated Using an Electrospinning Technique. Ind Eng Chem Res 2017;56:12596–607. https://doi.org/10.1021/acs.iecr.7b02622.

[140] Ramasundaram S, Yoon S, Kim KJ, Park C. Preferential formation of electroactive crystalline phases in poly(vinylidene fluoride)/organically modified silicate nanocomposites. J Polym Sci Part B Polym Phys 2008;46:2173–87. https://doi.org/10.1002/polb.21550.

[141] Lopes AC, Costa CM, Tavares CJ, Neves IC, Lanceros-Mendez S. Nucleation of the electroactive γ phase and enhancement of the optical transparency in low filler content poly(vinylidene)/clay nanocomposites. J Phys Chem C 2011;115:18076–82. https://doi.org/10.1021/jp204513w.

[142] Yoon K, Kelarakis A. Nanoclay-directed structure and morphology in PVDF electrospun membranes. J Nanomater 2014;2014. https://doi.org/10.1155/2014/367671.

[143] Xin Y, Qi X, Tian H, Guo C, Li X, Lin J, et al. Full-fiber piezoelectric sensor by straight PVDF/nanoclay nanofibers. Mater Lett 2016;164:136–9. https://doi.org/10.1016/j.matlet.2015.09.117.

[144] Khalifa M, Mahendran A, Anandhan S. Probing the synergism of halloysite nanotubes and electrospinning on crystallinity, polymorphism and piezoelectric performance of poly(vinylidene fluoride). RSC Adv 2016;6:114052–60. https://doi.org/10.1039/C6RA20599B.

[145] Tiwari S, Gaur A, Kumar C, Maiti P. Enhanced piezoelectric response in nanoclay induced electrospun PVDF nanofibers for energy harvesting. Energy 2019;171:485–92. https://doi.org/10.1016/j.energy.2019.01.043.

[146] Li L, Zhang M, Rong M, Ruan W. Studies on the transformation process of PVDF from α to β phase by stretching. RSC Adv 2014;4:3938–43. https://doi.org/10.1039/c3ra45134h.

[147] Gade H, Bokka S, Chase GG. Polarization treatments of electrospun PVDF fiber mats. Polymer (Guildf) 2021;212:123152. https://doi.org/10.1016/j.polymer.2020.123152.

[148] Sarkar K, Ghalia M Ben, Wu Z, Bose SC. A neural network model for the numerical prediction of the diameter of electro-spun polyethylene oxide nanofibers. J Mater Process Technol 2009;209:3156–65. https://doi.org/10.1016/j.jmatprotec.2008.07.032.

[149] Saadeh W, Tekeste T, Perrott MH. A > 89% efficient LED driver with 0.5V supply voltage for applications requiring low average current. Proc 2013 IEEE Asian Solid-State Circuits Conf A-SSCC 2013 2013:273–6. https://doi.org/10.1109/ASSCC.2013.6691035.

[150] Pistoia G. Battery operated devices and systems: From portable electronics to industrial products 2008.

[151] Khedri M, Beheshtizadeh N, Rostami M, Sufali A, Rezvantalab S, Dahri M, et al. Artificial Intelligence Deep Exploration of Influential Parameters on Physicochemical Properties of Curcumin-Loaded Electrospun Nanofibers. Adv NanoBiomed Res 2022;2100143:2100143. https://doi.org/10.1002/anbr.202100143.

[152] Song J, Yang B, Zeng W, Peng Z, Lin S, Li J, et al. Highly Flexible , Large-Area , and Facile Textile-Based Hybrid Nanogenerator with Cascaded Piezoelectric and Triboelectric Units for Mechanical Energy Harvesting. Adv Mater Technol 2018;3:1800016.

https://doi.org/10.1002/admt.201800016.

[153] Sabry RS, Hussein AD. PVDF: ZnO/BaTiO3 as high out-put piezoelectric nanogenerator. Polym Test 2019;79. https://doi.org/10.1016/j.polymertesting.2019.106001.

[154] Trupp FJ, Cibils R, Goyanes S. Poly (vinylidene fluoride) electrospun nonwovens morphology: Prediction and optimization of the size and number of beads on fibers through response surface methodology and machine learning regressions. J Ind Text 2022;51:9071S-9096S.

[155] Methods C, Mech A. An energy approach to the solution of partial differential equations in computational mechanics via machine learning : Concepts , implementation and applications. Comput Methods Appl Mech Eng 2020;362:112790. https://doi.org/10.1016/j.cma.2019.112790.

[156] Hwang SH, Song JY, Ryu H Il, Oh JH, Lee S, Lee D, et al. Adaptive Electrospinning System Based on Reinforcement Learning for Uniform-Thickness Nanofiber Air Filters. Adv Fiber Mater 2023:1–15.